OPEN ACCESS Freely available online

PLoS one

An *In Vitro* Model for Lewy Body-Like Hyaline Inclusion/ Astrocytic Hyaline Inclusion: Induction by ER Stress with an ALS-Linked SOD1 Mutation

Satoru Yamagishi[1,2*☯¤a], Yoshihisa Koyama[1,2☯], Taiichi Katayama[1,2☯¤b], Manabu Taniguchi[1,2], Junichi Hitomi[1,2], Masaaki Kato[3], Masashi Aoki[3], Yasuto Itoyama[3], Shinsuke Kato[4*], Masaya Tohyama[1,2]

1 Department of Anatomy and Neuroscience, Graduate School of Medicine, Osaka University, Suita, Osaka, Japan, 2 The 21st Century Center of Excellence Program, Graduate School of Medicine, Osaka University, Suita, Osaka, Japan, 3 Department of Neurology, Tohoku University School of Medicine, Sendai, Japan, 4 Department of Neuropathology, Institute of Neurological Sciences, Faculty of Medicine, Tottori University, Yonago, Japan

Neuronal Lewy body-like hyaline inclusions (LBHI) and astrocytic hyaline inclusions (Ast-HI) containing mutant Cu/Zn superoxide dismutase 1 (SOD1) are morphological hallmarks of familial amyotrophic lateral sclerosis (FALS) associated with mutant SOD1. However, the mechanisms by which mutant SOD1 contributes to formation of LBHI/Ast-HI in FALS remain poorly defined. Here, we report induction of LBHI/Ast-HI-like hyaline inclusions (LHIs) *in vitro* by ER stress in neuroblastoma cells. These LHI closely resemble LBHI/Ast-HI in patients with SOD1-linked FALS. LHI and LBHI/Ast-HI share the following features: 1) eosinophilic staining with a pale core, 2) SOD1, ubiquitin and ER resident protein (KDEL) positivity and 3) the presence of approximately 15–25 nm granule-coated fibrils, which are morphological hallmark of mutant SOD1-linked FALS. Moreover, in spinal cord neurons of L84V SOD1 transgenic mice at presymptomatic stage, we observed aberrant aggregation of ER and numerous free ribosomes associated with abnormal inclusion-like structures, presumably early stage neuronal LBHI. We conclude that the LBHI/Ast-HI seen in human patients with mutant SOD1-linked FALS may arise from ER dysfunction.

Citation: Yamagishi S, Koyama Y, Katayama T, Taniguchi M, Hitomi J, et al (2007) An *In Vitro* Model for Lewy Body-Like Hyaline Inclusion/Astrocytic Hyaline Inclusion: Induction by ER Stress with an ALS-Linked SOD1 Mutation. PLoS ONE 2(10): e1030. doi:10.1371/journal.pone.0001030

INTRODUCTION

Amyotrophic lateral sclerosis (ALS) is a progressive neurodegenerative disorder in which both upper and lower motor neurons begin to degenerate in middle-aged persons. About 10% of ALS patients demonstrate autosomal dominant inheritance of this disease, a disorder known as familial ALS (FALS) [1–6]. About 20% of FALS cases are associated with mutations of the Cu/Zn-superoxide dismutase (SOD1) gene [7]. SOD1 is an abundant protein of approximately 153 amino acids that accounts for approximately 1% of total cytosolic protein. More than 100 different SOD1 mutations have been reported as risk factors in association with FALS.

The endoplasmic reticulum (ER) is responsible for the synthesis, initial post-translational modification, and proper folding of proteins, as well as for their sorting export and delivery to appropriate cellular destinations. A variety of conditions, such as loss of the intraluminal oxidative environment or loss of calcium homeostasis, can cause accumulation of misfolded proteins in the ER. To cope with such accumulation, there are three possible responses in eukaryotes. The first response is known as the unfolded protein response (UPR), in which IRE1α and ATF6 recognize aberrant proteins and increase the expression of ER-resident chaperones such as GRP78/BiP and GRP94 to promote proper protein folding [8,9]. The second response involves suppression of translation mediated by the serine/threonine kinase PERK, which phosphorylates and inactivates the translation initiation factor eIF-2α to reduce the production of misfolded proteins [10,11]. The third response is ER-associated degradation (ERAD), in which misfolded proteins are expelled from the ER and targeted for degradation by cytoplasmic proteasomes [12,13]. Although these three protective responses can transiently control the accumulation of misfolded proteins within the ER, they can be overcome by sustained 'ER stress' [14–16]. 'ER stress' is involved in neuronal death and various neurodegenerative disorders, such as Charcot-Marie-Tooth disease, and is especially related to inclusion body diseases such as Alzheimer's disease, Parkinson's disease, Huntington's disease and ALS [17–23].

Histopathologic studies have revealed that neuronal Lewy body-like hyaline inclusions (LBHI) and astrocytic hyaline inclusions (Ast-HI), are morphological hallmarks of mutant SOD1-linked FALS [24]. Neuronal LBHI and Ast-HI are ultrastructually identical and share various features, with both consisting of 15–25 nm granule-coated fibrils, both showing immunoreactivity for

Academic Editor: Xiao-Jiang Li, Emory University, United States of America

Received February 28, 2007; **Accepted** September 23, 2007; **Published** October 10, 2007

Funding: This work was supported in part by a grant from the 21st Century COE Program, Japan Society for the Promotion of Science, 6 Ichibancho, Chiyoda-ku, Tokyo 102-8471, Japan, a Grant-in-Aid for Scientific Research (c) from the Ministry of Education, Culture, Sports, Science and Technology of Japan (S.K.: 17500229), a Grant from Research on Psychiatric and Neurological Disease and Mental Health (SK, MA, YI) and a Research Grant on Measures for Intractable Diseases from the Ministry of Health, Labour and Welfare of Japan (SK, YI). SY is supported by a long-term fellowship by European Molecular Biology Organization (EMBO) and Japan Society for the Promotion of Science (JSPS).

Competing Interests: The authors have declared that no competing interests exist.

* **To whom correspondence should be addressed.** E-mail: yamagishi@neuro.mpg.de (SY); kato@grape.med.tottori-u.ac.jp (SK)

☯ These authors contributed equally to this work.

¤a **Current address:** Molecular Neurobiology, Max-Planck-Institute of Neurobiology, Martinsried, Munich, Germany,
¤b **Current address:** Department of Anatomy and Neuroscience, Hamamatsu University School of Medicine, Hamamatsu, Shizuoka, Japan

SOD1, ubiquitin, and copper chaperone for SOD (CCS), and both appearing late in the course of the disease (i.e. at ~10 to 30 years of age in humans [24–27]). Recently, Wate et al. reported that neuronal LBHI are immunoreactive for GRP78/BiP, a component of the UPR cellular response to ER stress [28].

In the present study, we show that ER stress in a neuroblastoma line expressing mutant SOD1 can provoke SOD1 aggregation in ER and formation of LBHI/Ast-HI-like hyaline inclusion bodies (LHIs), which show SOD1, ubiquitin, GRP78/BiP and ER resident protein (KDEL) immunopositivity similar to the shared cytopathological features of LBHI and Ast-HI. Induced neuroblastoma LHI furthermore consisted of 15–25 nm granule-coated fibrils, a hallmark of mutant SOD1-linked FALS, raising the possibility that these acutely induced aggregations represent a precursor to LBHI/Ast-HI seen in advanced FALS. In support of this possibility, we observe abnormal ER and numerous free ribosomes aggregated in the peri-nuclear region neuroblastoma cells expressing L84V SOD1 under ER stress condition and in spinal cord neurons in presymptomatic transgenic mice expressing L84V SOD1. Taken together, these findings suggest a model for early events in FALS cellular pathology, in which ER stress promotes the aggregation of mutant SOD1 and is involved in the development of LBHI/Ast-HI in patients with mutant SOD1 linked FALS.

RESULT

Aggregation and ubiquitination of mutant SOD1 under ER stress

To identify conditions which lead to the aggregation of mutant SOD1, we generated SK-N-SH human neuroblastoma cell lines that stably expressed FLAG-tagged human SOD1 encoding a leucine to valine substitution mutation (L84V) associated with FALS [29]. Western blot analysis confirmed that expression of endogenous and exogenous SOD1 was equal in the cell line (Fig. 1A). Reports that neuronal LBHI contain GRP78/BiP, an ER resident component of the UPR response, suggested that ER stress might be a factor in the aggregation of mutant SOD1 [28]. We therefore examined localization of wild-type and mutant SOD1 under normal conditions and under conditions of ER stress (Figure 1). Under normal conditions, wild-type and L84V SOD1 were distributed through the cytosol (Fig. 1B and D). However, following treatment with tunicamycin, an inhibitor of N-glycosylation which causes ER stress, small SOD1-positive aggregates (up to 3 μm in diameter) were seen in L84V SOD1-expressing cells (22.3%, $p<0.001$; Fig. 1E and F). A much smaller percentage of wild-type SOD1 expressing cells (2.9%, n.s.) showed non-inducible SOD1 aggregation (Fig. 1C and F). To confirm whether ER stress is required for the aggregation of SOD1, we compared tunicamycin and thapsigargin as ER stress inducers with etoposide as a non-ER stress inducer (causing DNA damage). Exposure to 1 and 3 μg/ml tunicamycin (21.1% and 17.5%, respectively) or 0.3 and 1 μM thapsigargin (27.0% and 27.2%, respectively) significantly increased the number of cells containing SOD1 aggregates, in L84V SOD1 expressing neuroblastoma cells. Treatment with 100 and 300 μM etoposide did not lead to a significant increase in aggregates (Fig. 1G). Thus mutant SOD1 forms aggregates following treatments provoking ER stress, but not following treatment causing damage to the nucleus.

Since the SOD1-positive inclusions of FALS patients are known to be eosinophilic [26], we performed hematoxylin-eosin (HE) and anti-SOD1 antibody staining to determine whether the aggregates induced in the neuroblastoma line were also eosinophilic.

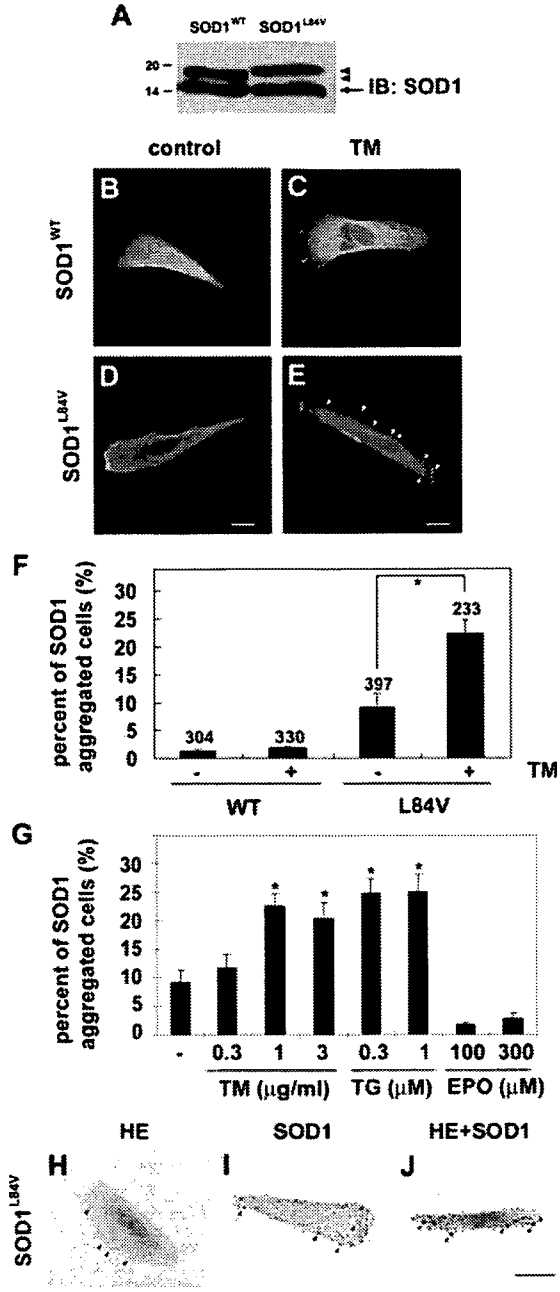

Figure 1. Eosinophilic aggregates of L84V SOD1 are induced by ER stress. (A) Western blotting analysis of the expression of SOD1 in SK-N-SH cells, which stably expressed FLAG tagged wild-type SOD1 or L84V mutant SOD1. Arrowheads and arrow indicate exogenous and endogenous SOD1, respectively. (B–D) Immunofluorescent analysis of SOD1 aggregates in SK-N-SH cells expressing wild-type SOD1 (B, C) or L84V SOD1 (D, E). Cells were incubated under control conditions (B, D) or with 1 μg/ml tunicamycin (C, E) for 24 h, and then were fixed and stained with an anti-SOD1 antibody. Tunicamycin induced aggregates of SOD1 (arrowheads) in L84V SOD1-expressing cells, but not in wild-type SOD1-expressing cells. Scale bar = 20 μm. (F) Quantification of (B-D). After the staining the cells with SOD1 aggregates were counted and scored. Numbers indicate the amounts of total counted cells. Asterisks show a significant difference from control, *$p<0.001$. (G) SOD1 aggregates induced by tunicamycin and thapsigargin, but not by etoposide. SK-N-SH cells expressing L84V SOD1 were exposed to 0.3, 1 and 3 μg/ml tunicamycin, 0.3 and 1 μM thapsigargin and 100 and 300 μM etoposide. Asterisks show a significant difference from control, *$p<0.001$. (H-J) Eosinophilic SOD1 aggregates induced by tunicamycin. Cells were treated as described in (E) and then stained with HE (H), anti-SOD1 antibody (I), or both (J). Scale bar = 20 μm.
doi:10.1371/journal.pone.0001030.g001

Figures 1H–J show that the aggregates induced by tunicamycin treatment were positive for both eosin and SOD1.

In patients with mutant SOD1-linked FALS, SOD1-positive aggregates are reported to be ubiquitinated by RING finger-type E3 ubiquitin ligases such as dorfin [30–33]. To investigate whether the SOD1 aggregates induced by ER stress were ubiquitinated, we performed double immunostaining with anti-SOD1 and anti-ubiquitin antibodies (Fig. 2 A–R). After treatment with either tunicamycin or ALLN, a specific proteasome inhibitor, wild-type and L84V SOD1-expressing cells were immunostained with anti-SOD1 and anti-ubiquitin antibodies. As a result, mutant SOD1 aggregates induced by either tunicamycin or ALLN were clearly colocalized with ubiquitin, suggesting the SOD1 were ubiquitinated. To further examine the ubiquitination of the mutant SOD1, a co-immunoprecipitation assay utilizing ubiquitin was performed (Fig. 2S). As expected, L84V SOD1-expressing cells showed a positive ubiquitin ladder after ALLN treatment, but wild-type SOD1-expressing cells did not.

Aggregates of SOD1 show positive localization to the ER, but not to the mitochondria, lysosomes, or Golgi apparatus

Under normal conditions, SOD1 is diffusely distributed throughout the cytoplasm. In contrast, under the pathological condition, SOD1 aggregates are associated with specific organelles such as the mitochondria and/or ER [34–37]. Since the tunicamycin-induced aggregates of mutant SOD1 were localized to the central and peripheral regions of the cytoplasm (Fig. 1E, H–J), we investigated the subcellular localization of these aggregates with organelle specific markers. Confocal microscopy analysis clearly showed colocalization of SOD1 and an ER retention signal

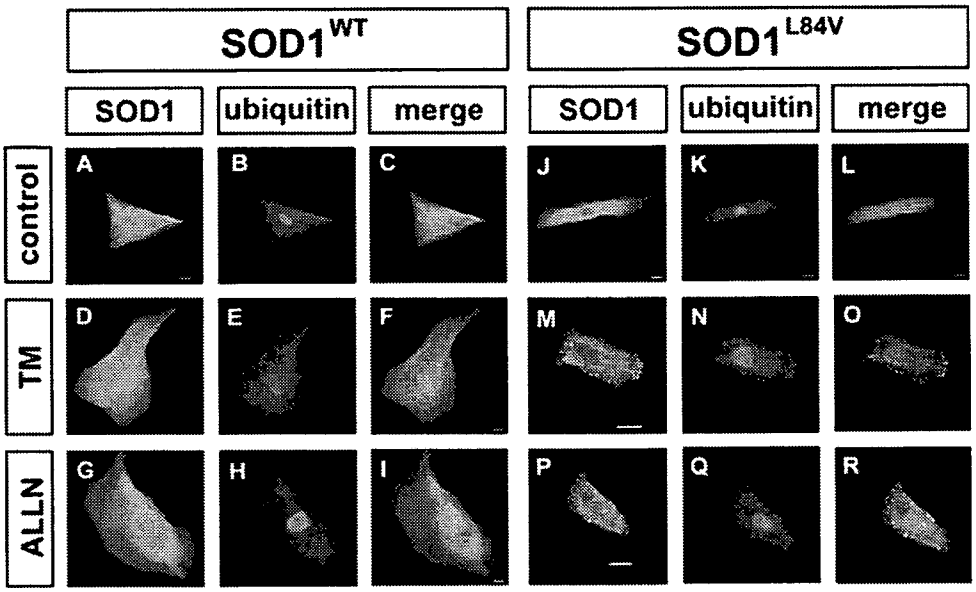

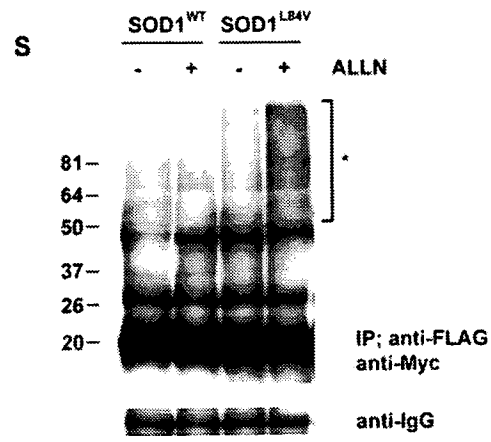

Figure 2. Ubiquitination of mutant SOD1 aggregates. (**A–R**) Colocalization assay with SOD1 and ubiquitin. SK-N-SH cells expressing wild-type SOD1 (**A–I**) or L84V SOD1 (**J–R**) were incubated with 1 μg/ml of tunicamycin (**D–F, M–O**), 4 μg/ml of ALLN (**G–I, P–R**), or no agents (**A–C, J–L**) for 24 h. Then the cells were fixed and stained with anti-SOD1 antibody (green; **A, D, G, J, M, P**) or anti-ubiquitin antibody (red; **B, E, H, K, N, Q**). Arrows indicate colocalization of SOD1 aggregates and ubiquitin. Scale bar = 20 μm. (**S**) Co-immunoprecipitation assay utilizing ubiquitin. SK-N-SH cells stably expressing wild-type and L84V SOD1 were transfected with a myc-tagged ubiquitin expression vector. After incubation with or without ALLN, cell lysates were prepared and assayed with anti-myc antibody of the immunoprecipitant with anti-FLAG antibody. Asterisk shows an ubiquitinated ladder that appeared after ALLN treatment of L84V SOD1-expressing cells. IgG bands are shown as loading controls.
doi:10.1371/journal.pone.0001030.g002

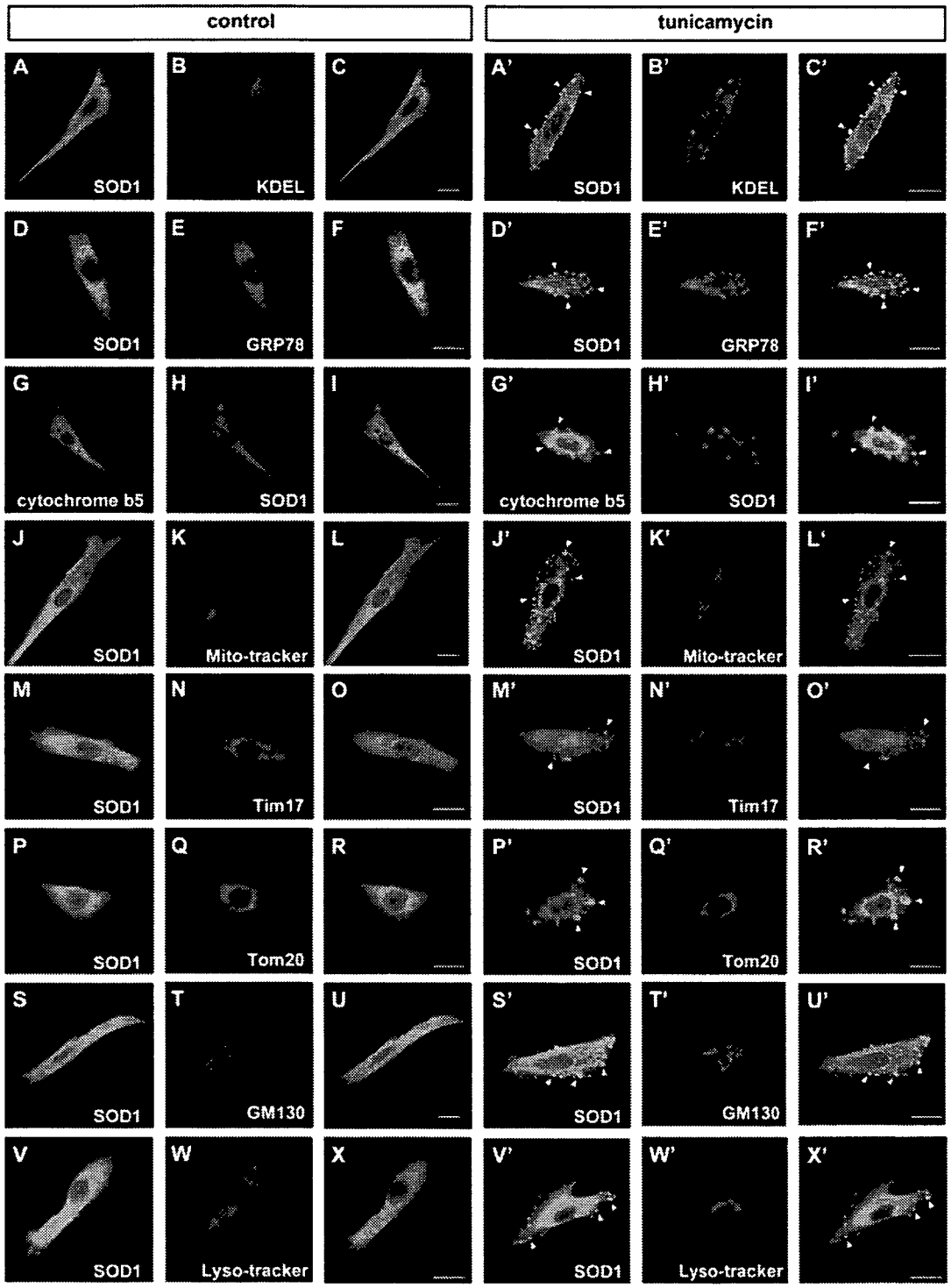

Figure 3. Positive translocation of SOD1 aggregates to ER, but not to the mitochondria, Golgi apparatus, or lysosomes. (**A–I, A'–I'**) Stress-dependent localization of SOD1 to the ER. L84V SOD1-expressing SK-N-SH cells were incubated for 24 h without (**A–I**) or with 1 μg/ml of tunicamycin (**A'–I'**). Then the cells were fixed and stained using an anti-SOD1 antibody (green; **A, D, A', D'**) and an anti-KDEL antibody (red; **B, B'**) or an anti-GRP78/BiP antibody (red; **E, E'**). GFP-cytochrome b5 were transfected to the cells and stained with anti-GFP (green; **G, G'**) and anti-SOD1 (red; **H, H'**) antibodies. Merged images (**C, F, I, C' F', I'**). The aggregates of SOD1 (arrowheads) are positive for KDEL, GRP78/BiP and cytochrome b5. (**J–R, J'–R'**) Analysis of SOD1 localization to the mitochondria. L84V SOD1-expressing SK-N-SH cells were treated as described in above. The locations of the mitochondria and SOD1 were visualized in L84V SOD1-expressing SK-N-SH cells using 100 nM Mito-tracker (red; **K, K'**), an anti-Tim17 antibody (red; **N, N'**) or an anti-Tom20 antibody (red; **Q, Q'**) and an anti-SOD1 antibody (green; **J, M, P, J', M', P'**). Merged images (**L, O, R, L', O', R'**). (**S–U, S'–U'**) Investigation of SOD1 localization to the Golgi apparatus. L84V SOD1-expressing SK-N-SH cells were treated as described in above. Then the cells were stained with anti-SOD1 antibody (green; **S, S'**) and anti-GM130 antibody (red; **T, T'**). Merged images (**U, U'**). (**V-X, V'-X'**) Analysis of the localization of SOD1 to the lysosomes. A GFP-tagged L84V SOD1 vector was transfected into L84V SOD1-expressing SK-N-SH cells. After 24 h of incubation with 1 μg/ml of tunicamycin, the cells were incubated for a further 30 min with 100 nM Lyso-tracker (red; **W, W'**) to visualize the lysosomes. GFP channel (**V, V'**) Merged images (**X, X'**). Scale bars = 20 μm. Arrowheads indicate aggregated SOD1.
doi:10.1371/journal.pone.0001030.g003

(KDEL) containing protein and GRP78/BiP, suggesting SOD1 localization in ER (Fig. 3A–F, A′–F′). In order to confirm the SOD1 colocalization with ER, we utilized GFP conjugated cytochrome b5, a typical C-terminal anchored ER membrane protein. As expected, SOD1 showed the positive staining with cytochrome b5, indicating mutant SOD1 localization to ER (Fig. 3G–I, G′–I′). In the absence of stress, ER was located to the perinuclear region. However, treatment with tunicamycin seemed to cause its relocation to an abnormal region near the cell periphery. The aberrant distribution of ER following tunicamycin treatment was not observed in cells expressing wild type SOD1 (Fig. S1C′, F′ and I′). These results suggest deterioration of ER function and localization due to aggregation of mutant SOD1.

In light of previous reports identifying mutant SOD1 colocalization to the mitochondria [34,35,37], we also examined the potential colocalization of mutant SOD1 with mitochondria. In contrast to the results with markers for ER, the SOD1 aggregates induced by tunicamycin did not colocalize with the mitochondria marker Mitotracker, with Tim17 which marks the mitochondrial inner membrane nor Tom20 which marks the mitochondrial outer membrane (Fig. 3J′–R′). The localization of these SOD1 aggregates also did not correspond with the Golgi apparatus or the lysosomes, which were stained by anti-GM130 antibody and Lyso-tracker, respectively (Fig. 3S′–X′).

Our previous results in figure 3C′, F′ and I′ revealed aberrant redistribution of ER membranes in tunicamycin-treated mutant SOD1 expressing cells to the cell periphery region. To directly visualize the localization of ER, we performed electron microscopic analysis of tunicamycin-stressed cells expressing mutant SOD1. Figure 4A and B showed abnormal aggregates of rough ER, sac-like structures with surface ribosomes, associated with numerous free ribosomes. Mutant SOD1 localization to these peripheral aggregates was confirmed by immunoelectron microscopy (Fig. 4C), implying defective functional activities of ER and free ribosomes in cells expressing mutant SOD1.

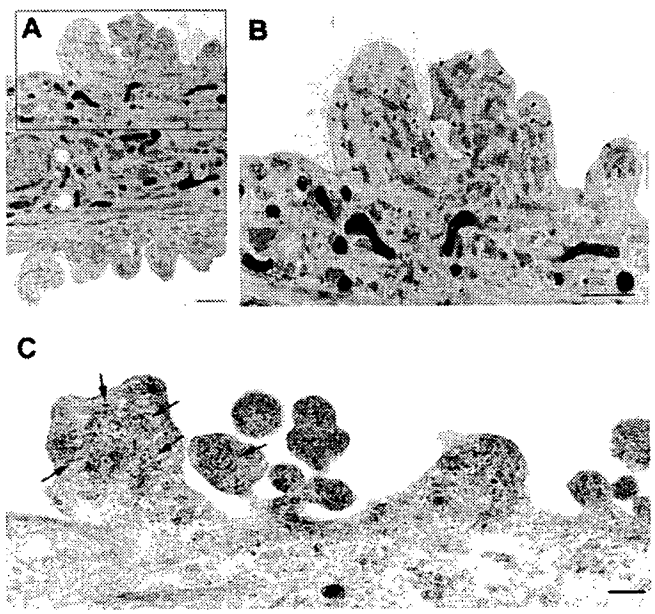

Figure 4. ER and SOD1 co-localization in peri-cytoplasmic membrane region. (A) Electron micrograph of L84V SOD1-expressing SK-N-SH cells after treatment with 1 μg/ml of tunicamycin for 24 h as described in Materials and Methods. (B) Enlargement of part of (A). Arrowheads indicate abnormal ER aggregates, where mutant SOD1 is localized as in Fig. 3C′ and 3E′. Scale bar = 1 μm. (C) SOD1 localization in peri-cytoplasmic membrane region. Cells were treated as described in (A) and immune electron micrograph was obtained as described in Materials and Methods. Arrows show SOD1 immunoreactive in ER.
doi:10.1371/journal.pone.0001030.g004

LBHI/Ast-HI-like Inclusions are induced by ER stress.

Wate et al. [28] reported that neuronal LBHI in G93A SOD1 transgenic mice are immune reactive for GRP78/BiP, an ER resident component of the UPR response. As shown in figures 3A′-I′ and 4C, mutant SOD1 localized to the ER following stress induction by tunicamycin. These SOD1 aggregates shared additional features with LBHI/Ast-HI, namely eosin positivity and ubiquitin immune reactivity. Those observations led us to consider whether ER stress would eventually induce the formation of full-fledged LBHI/Ast-HI. To test this hypothesis, we examined whether inclusion bodies containing mutant SOD1 developed in L84V SOD1-expressing cells subjected to ER stress. Consistent with this idea, eosinophilic hyaline inclusions (~10 to 20 μm in diameter) with a pale core, which are similar to neuronal LBHI/Ast-HI in the spinal cord of ALS patients harboring a SOD1 mutation, developed within 24 hrs of exposure to tunicamycin (Fig. 5A), but not in cells expressing wild type SOD1 (data not shown). In fact, the eosin-positive LBHI/Ast-HI-like hyaline inclusions (LHIs) were morphologically similar to the Ast-HI seen in the spinal cord of transgenic L84V SOD1 mice at the symptomatic stage (Fig. 5A and D). Furthermore, ultrastructual analysis revealed that the LHIs in neuroblastoma cells were composed of granule-coated fibrils (approximately 15–25 nm in diameter) and granular materials, which are the typical morpho-

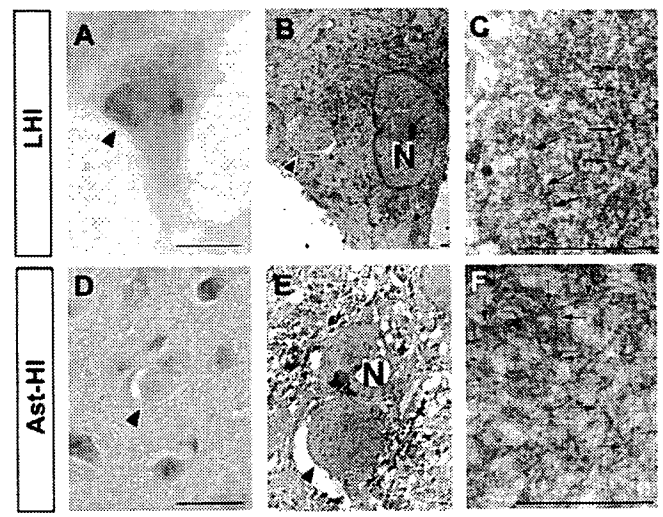

Figure 5. LHIs containing granule-coated fibrils are morphologically identical with Ast-HI from L84V transgenic mice. (A–F) Comparison of a LHI induced by ER stress in an L84V SOD1-expressing SK-N-SH cell (A–C) and Ast-HI in the spinal cord of a transgenic L84V SOD1 mouse (D–F). (A) An eosinophilic LHI in the cytoplasm of the SK-N-SH cell expressing L84V SOD1 cell was induced by treatment with 1 μg/ml of tunicamycin for 24 h (scale bar = 20 μm). (B) Electron micrograph of a hyaline inclusion (arrow) obtained by the direct epoxy resin-embedding method after decolorization of the HE-stained section shown in (A). N, nucleus; ×3000 (scale bar = 1 μm). (C) At a high magnification, the inclusion is composed of granule-coated fibrils (arrows) approximately 15–25 nm in diameter and granular materials. ×16000 (scale bar = 1 μm). (D) An eosinophilic Ast-HI from a transgenic L84V SOD1 mouse. (E) Electron micrograph of an Ast-HI obtained by the direct epoxy resin-embedding method mentioned in (B). N, nucleus; ×2000 (scale bar = 1 μm). (F) Enlargement of (E). ×16000 (scale bar = 1 μm). Note that the fibrils observed in (C) and (F) are ultrastructually identical.
doi:10.1371/journal.pone.0001030.g005

logical hallmarks of mutant SOD1-linked FALS, and were identical with the Ast-HI found in L84V SOD1 mice (Fig. 5C, F; [38]). These results suggest that LBHI/Ast-HI in FALS patients might be provoked by ER stress as we observed for LHIs.

We further explored the molecular similarity between the LHI and LBHI/Ast-HI, using double-label immunocytochemistry. As shown in figure 6A–D, LHIs induced by tunicamycin are immunopositive for anti-SOD1 and anti-ubiquitin antibodies, consistent with the LBHI/Ast-HI features. In the spinal cord of G93A SOD1 mutant mice at the symptomatic stage, neuronal LBHI show GRP78/BiP immunoreactive, suggesting the involvement of ER resident protein [28]. Therefore, we examined whether LHIs also contain ER resident protein. As expected, LHI showed anti-KDEL positivity, indicating the involvement of ER resident proteins such as calreticulin, GRP 94, PDI and GRP78/BiP in LHI development (Fig. 6E and F). Furthermore, Ast-HI in spinal cord of L84V SOD1 transgenic mice at symptomatic stage also showed KDEL positive (Fig. 6G and H), meaning that the principle features of these inclusions in neuroblastoma cells and the LBHI/Ast-HI of FALS patients are the same and implying LHI and LBHI/Ast-HI might develop in similar procedure.

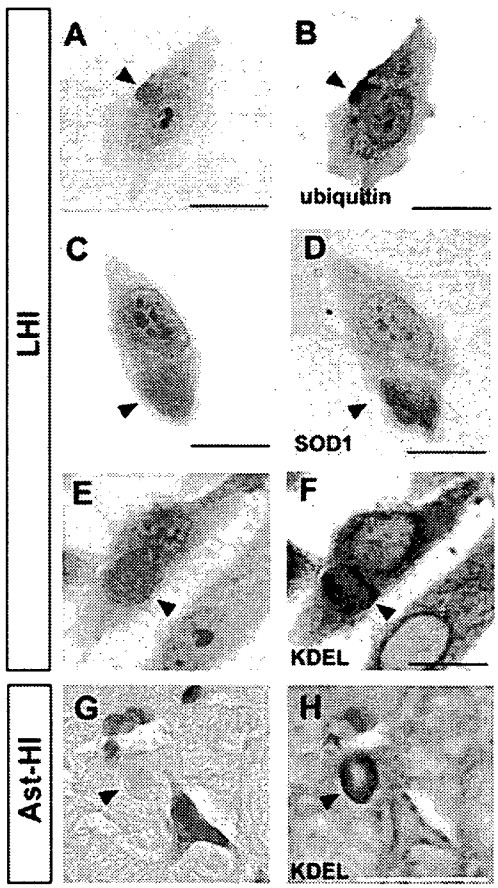

Figure 6. Positive immunoreactive against ubiquitin, SOD1 and KDEL of LHIs. (A–D) LHIs show immunoreactive against ubiquitin and SOD1. Eosinophilic LHIs in SK-N-SH cells (arrowheads in A and C) induced by tunicamycin were immunostained for ubiquitin (B) and SOD1 (D) after de-colorization. (E–H) KDEL immunoreactive in both LHI and Ast-HI. Eosinophilic LHI in SK-N-SH cells (arrowhead in E) and Ast-HI in spinal cord of L84V SOD1 mouse (arrowhead in G) were immunostained against anti-KDEL antibody after de-colorization (F, H). Scale bar = 20 μm

doi:10.1371/journal.pone.0001030.g006

Abnormal ER aggregated around peri-nuclear region with numerous free ribosomes at presymptomatic stage of Ast-HI in L84V SOD1 mice.

To further explore the relationship of LHI to the development of LBHI/Ast-HI in FALS patients with mutant SOD1, we performed ultrastructual examination of transgenic L84V SOD1 mice, which show neuronal LBHI and Ast-HI at symptomatic stage (Fig. 5D–F, 6G–H; [35]). We examined the mice at the presymptomatic stage in the hope of detecting precursors to hyaline inclusion bodies. In spinal cord neurons of the pre-symptomatic L84V SOD1 transgenic mice, we observed aberrant aggregation of electron-dense rough ER around the peri-nuclear region with numerous free ribosomes, which were suspected to be producing mutant SOD1 (Fig. 7). This suggests that the aberrant SOD1 fibrils observed in spinal neurons of these mice at later

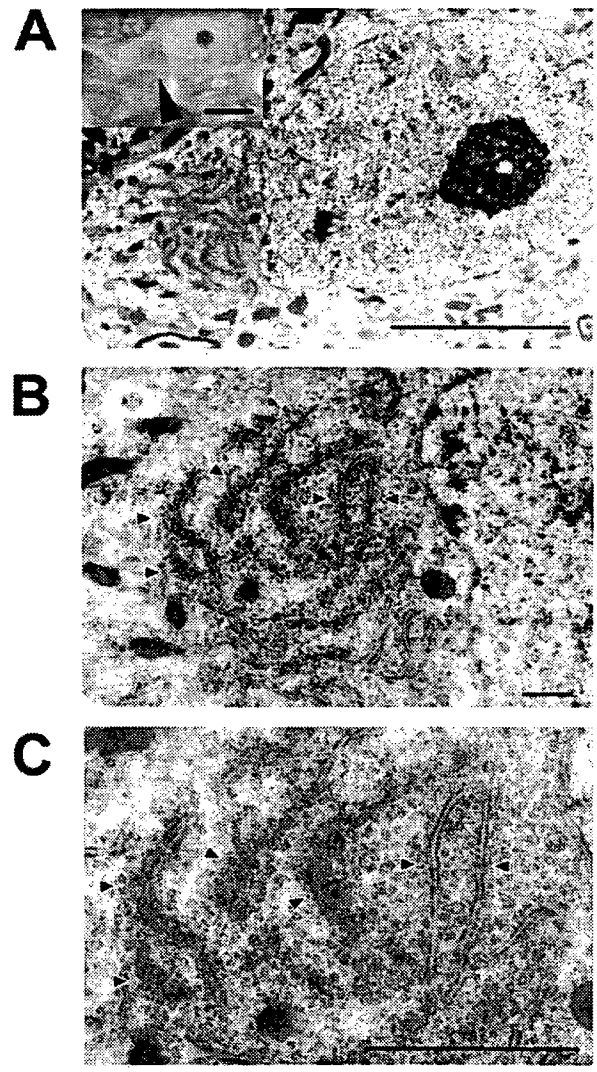

Figure 7. ER shows abnormal aggregation with numerous free ribosomes in L84V SOD1 mouse at presymptomatic stage. (A–C) Electron micrographs of a neuron obtained from an L84V SOD1 transgenic mouse containing ER aggregates. The inset in (A) shows a cytoplasmic inclusion-like structure (arrowhead) stained with toluidine blue. (A) ×3500 (scale bars = 20 μm). (B) ×8000 (scale bar = 1 μm). (C) ×15000 (scale bar = 1 μm). Arrowheads indicate abnormal ER aggregates.

doi:10.1371/journal.pone.0001030.g007

stages might be produced by cooperative activity of ER and ribosomes. These inclusion-like structures with abnormal accumulation of ER seemed likely to represent a precursor to the later neuronal LBHI observed in this line. These results imply that the deterioration of ER function and the involvement of ER might be important for formation and developing neuronal LBHI/Ast-HI in mutant SOD1 harboring FALS patients.

DISCUSSION

Aggregated proteins or inclusions are a pathological hallmark and possible causative agent of several neurodegenerative disorders including ALS [39]. While LBHI/Ast-HI have been established as morphological hallmarks of mutant SOD1-linked FALS, little is known about the formation of these structures in neurons [6]. Several in vitro systems have been provided for analysis mutant SOD1 aggregation [35,36,40], however, the relationship between mutant SOD1 aggregation *in vitro* and pathological hyaline inclusions *in vivo* remains unclear. The LHI we observed in SK-N-SH cells expressing mutant SOD1 provide a direct link between *in vitro* and *in vivo* SOD1 aggregation. To our knowledge, this is the first study to show reproducible induction of LBHI/Ast-HI like structures meeting the criteria of inclusion bodies [24,26,31,38,41].

LBHIs/Ast-HIs in human FALS consist of a chaotic mixture of cytoplasmic proteins (such as SOD1, copper chaperone for SOD (CCS), peroxiredoxin 2, and glutathione peroxidase 1), cytoskeletal proteins (such as tubulin, tau protein, and phosphorylated- and nonphosphorylated neurofilament), nuclear proteins (such as neuron-specific enolase) and synaptic proteins (such as synaptophysin [24,38,41–43]). Recently, it has been published that GRP78/BiP, an ER resident chaperon protein, is also co-localized with LBHI of G93A SOD1 mice [28]. GRP78/BiP is molecular chaperone protein induced by IRE1 in response to aberrant protein folding and promotes proper protein folding. In this context, GRP78/BiP may be acting as part of the UPR response to resolve granule coated fibrils. Tobisawa et al. [35] reported increased protein levels of GRP78/BiP in motor neurons of mutant SOD1 transgenic mice, suggesting that the motor neurons in their model suffer from 'ER stress'. While the importance of ER stress or proteosome malfunction in formation of mutant SOD1 aggregates has been established [35,36,40], the mechanisms by which mutant SOD1 forms LBHI/Ast-HI in FALS remain poorly understood. In this study, we present three lines of evidence for the involvement of ER stress in early events in LBHI/Ast-HI formation. First, ER stress in neuroblastoma cells expressing mutant SOD1 results in SOD1- and ubiquitin-immunopositive LHIs, compatible with LBHI/Ast-HI, composed of granule-coated fibrils approximately 15–25 nm in diameter and granular materials (Figs. 5 and 6). Secondly, we observed similar structures in the spinal cord of L84V SOD1 transgenic mice at pre-symptomatic stages, including abnormal electron dense, i.e. stressed, ER and numerous free ribosomes. (Figs. 4 and 7). Third, positive staining against anti-KDEL antibody, which recognizes ER resident proteins such as calreticulin, GRP 94, PDI and GRP78/BiP, were observed in both the LHI and Ast-HI of L84V SOD1 transgenic mice at symptomatic stages (Fig. 6E–H). These findings support the hypothesis that ER stress induces LBHIs/Ast-HIs creation in FALS patients with mutant SOD1. Taken together, these observations suggest that LHI in neuroblastoma cells and LBHI/Ast-HI in FALS patients might develop through similar processes.

In this study, we presented evidences that ER stress causes aggregates of mutant SOD1 and formation of LHI which is compatible with LBHI/Ast-HI. However, other questions arise from these results. 1) Why did same stress induce the different outcome of mutant SOD1 aggregation in the neuroblastoma? 2) Are the smaller aggregates competent to develop to LHIs? To answer these questions, we sought without success to identify the origin of the granule coated fibrils or SOD1 containing filamentous structure (e.g. less densely coated fibrils) in the smaller SOD1 aggregates localized to ER in L84V SOD1 expressing cells. Nevertheless, we found common features between the small aggregates in L84V SOD1 expressing SK-N-SH cells and neuronal LBHI-precursor in L84V transgenic mice, including regions of abnormal ER aggregation surrounded by abundant free ribosomes (Fig. 4B and Fig 7C). Furthermore, LHI and Ast-HI were immunopositive for the KDEL peptide present in ER-resident proteins, suggesting the involvement of ER itself in formation or development of LBHI/Ast-HI (Fig. 6E–H). We suggest that aberrant SOD1 fibril might be produced by cooperative activity of ER and ribosomes. To answer the questions, careful observation of LHI with time lapse analysis is needed.

It remains unclear why the major symptoms of ALS in patients with mutant SOD1-linked FALS do not develop until middle age, but we speculate that age-dependent changes in responses to ER stress might provide an answer. Under normal conditions, newly synthesized and misfolded proteins are refolded by chaperons such as GRP78, 94, calnexin, and calreticulin. This UPR response may be more robust in younger FALS patients and might be the reason the proteins aggregates are not observed in young patients even though mutant SOD1 is expressed. However, a decrease in protein folding or chaperone capability may occur with aging, and accumulation of misfolded proteins in the ER lumen may gradually lead to ER stress [44]. Consistent with this idea, Tobisawa et al. reported mutant SOD1 retention in the ER in COS7 cells [35] and Kikuchi et al. reported age-dependent increase of mutant SOD1 aggregation to ER in spinal cord of G93A SOD1 mice, suggesting ER dysfunction might be caused by mutant SOD1 [36]. Prolonged ER stress associated with insufficient degradation of misfolded proteins would subsequently activate apoptotic pathways. Nakagawa et al. reported that caspase-12, the ER resident caspase, is specifically cleaved and activated by ER stress, and that cells derived from mice lacking caspase-12 are resistant to ER stress [16]. In the spinal cords of G93A SOD1 mice, caspase-12 is activated in symptomatic period and can be inhibited by overexpression of XIAP (X-linked inhibitor of apoptosis protein [45,46]. Then, we analyzed activation of caspase-4 (the human orthologue of rodent caspase-12) following tunicamycin treatment. As expected, the SOD1 aggregates of the L84V SOD1-expressing neuroblastoma cells colocalized with caspase-4 (unpublished data), implying caspase-4 might contribute to cell death in our model system.

Although it can take longer than 30 years for LBHI/Ast-HI to develop in FALS patients, we could induce the formation of morphologically similar LHI within 24 hours in our simple model. Detection of the molecular targets for ER stress-induced hyaline inclusions of mutant SOD1 in our model might lead to the development of therapy that can prevent the progression of mutant SOD1-linked FALS. Ultimately, our study should contribute to the development of a simple system to analyze novel therapies for ALS.

MATERIALS AND METHODS

Transgenic Mice

Transgenic mice for mutant human SOD1^{L84V} (C587BL/6 background) were created (M. Kato, et al. Transgenic mice with ALS-linked SOD1 mutant L84V. Abstract of the 31st Annual Meeting of Society for Neuroscience, San Diego, 2001). Mice were genotyped by PCR to detect the mutant SOD1 transgene using

the following primers: forward, TTGGGAGGAGGTAGTGATTA; reverse, GCTAGCAGGATAACAGATGA. The onset of symptoms was at 5–6 months and the initial sign of the disease was usually weakness in their hindlimbs, while approximately 10% of the mice first showed weakness in their forelimbs.

Chemicals and antibodies

We used the following antibodies: anti-SOD1 polyclonal antibody (pAb; Chemicon, Temecula, CA); anti-ubiquitin pAb and anti-KDEL mAb (Stressgen, Victoria, BC. Canada); anti-Tim17 pAb and anti-Tom20 pAb (grateful gifts by Dr. Otera and Prof. Mihara [47,48]); Alexa Fluor 488-conjugated anti-sheep IgG, Alexa Fluor 588-conjugated anti-mouse IgG antibody, and Alexa Fluor 588-conjugated anti-rabbit IgG antibody (Molecular Probes, Eugene OR); biotinylated anti-sheep IgG (Vector Laboratories, Burlingame, CA); anti-FLAG mAb (Sigma, woodlands, USA); anti-myc pAb and anti-GFP-mAb (Santa Cruz, Santa Cruz, CA); HRP-conjugated anti-sheep IgG (Jackson ImmunoResearch Laboratories Inc., West Grove, PA); and HRP-conjugated anti-mouse IgG and HRP-conjugated anti-rabbit IgG antibody (Cell Signaling Technology, Beverly, MA). Tunicamycin was obtained from Sigma.

Cell culture and induction of ER stress

SK-N-SH human neuroblastoma cells were obtained from the Riken Cell Bank (Tsukuba, Japan), and were cultured in α-MEM (Invitrogen) containing 10% fetal bovine serum at 37°C under 5% CO_2. These cells were transfected with pcDNA3.1-hSOD1 and pcDNA3.1-hL84V-SOD1 to cause overexpression of wild-type or L84V mutant SOD1, respectively. G418 resistant stable neuroblastoma cell lines expressing equal levels of endogenous and exogenous SOD1 were established. In all experiments, we used cultures that were at 70–80% confluence to avoid the influence of stress induced by overgrowth. On the day of stimulation, fresh medium was added more than 1 h before exposure to stress in order to ensure the same conditions for each culture.

Western blot analysis

SK-N-SH cells stably expressing wild-type or L84V SOD1 were washed with PBS, harvested, and lysed in TNE buffer containing 1 mM PMSF and 1% SDS. 10 μg of protein was subjected to 12% SDS-PAGE and transferred to a PVDF membrane (Millipore Corp.). The membrane was blocked with 5% skim milk and incubated with anti-SOD1 antibody (1:1500 dilution), followed by incubation with an HRP-conjugated secondary antibody. Proteins were visualized with an ECL detection system (Amersham-Pharmacia).

Immunocytochemistry

SK-N-SH cells stably expressing wild-type SOD1 or L84V SOD1 were treated with 1 μg/ml of tunicamycin for 24 h. Then the cells were fixed with Zamboni's solution (0.1 M phosphate-buffered saline (PBS; pH 7.4) containing 2% paraformaldehyde (PFA) and 21% picric acid), rinsed in 0.1 M PBS, and incubated for 30 min in 0.3% H_2O_2 to eliminate endogenous peroxidases. Next, the cells were incubated overnight at 4°C with the primary antibody (a polyclonal sheep anti-SOD1 antibody; Calbiochem) at 1:1000 in 0.1 M PBS containing 0.3% Triton X-100 and 3% bovine serum albumin (BSA). After washing in 0.1 M PBS, cells were incubated for 30 min with the secondary antibody (biotinylated anti-sheep IgG) (Vector Laboratories). After amplification with avidin-biotin complex from the ABC kit (Vector Laboratories), reaction products were visualized with 0.05 M Tris-HCl buffer (TBS; pH 7.6) containing 0.02% diaminobenzidine tetrahydrochloride (DAB) and 0.01% hydrogen peroxide. Finally, the cells were counterstained with Mayer's hematoxylin and eosin (HE).

Co-immunoprecipitation assay utilizing ubiquitin

Lysates of pcDNA3.1-myc-tagged ubiquitin (a kind gift from Dr. Niwa and Prof. Sobue [32])-transfected SK-N-SH cells stably expressing wild-type SOD1 or L84V SOD1 were prepared using TNE buffer (10 mM Tris-HCl, (pH 7.4), 150 mM NaCl, and 1 mM EDTA) containing 1 mM phenylmethylsulphonyl fluoride (PMSF), 2 μg/ml aprotinin, and 1% Nonidet P-40 after treatment with or without 4 μg/ml ALLN for 12 h. Then, 1 μg of anti-FLAG antibody was added to 400 μg of lysate, followed by incubation at 4°C for at least 3 h. Protein G-Sepharose (10 μl gel) was then added and incubation was done with rotation at 4°C for 1 h. The immunoprecipitate was subjected to SDS-PAGE and transferred to a polyvinylidene fluoride (PVDF) membrane. The membrane was blocked with 5% skim milk and then was incubated with anti-Myc antibody (1:1000 dilution), followed by incubation with an HRP-conjugated secondary antibody. Proteins were visualized with an ECL detection system (Amersham-Pharmacia).

Immunofluorescence and chemifluorescence

SK-N-SH cells expressing wild-type SOD1 or L84V SOD1 were incubated with or without tunicamycin or ALLN, rinsed in 0.02 M PBS, and fixed in Zamboni's fixative. Then the cells were incubated overnight at 4°C with an anti-SOD1 antibody (1:1000 dilution) and either anti-KDEL (1:500 dilution), anti-GM130 (1:500 dilution) or anti-ubiquitin (1:500 dilution) antibody in 0.02 M PBS containing 0.3% Triton X-100 and 3% BSA. Next, the cells were treated with fluorescent dye (Alexa Fluor 488)-conjugated donkey anti-sheep IgG (SOD1; 1:1000 dilution), fluorescent dye (Alexa Fluor 568)-conjugated goat anti-mouse IgG (KDEL, GM130; 1:1000 dilution), and goat anti-rabbit IgG (ubiquitin; 1:1000) as the secondary antibodies for 1 h at RT in 0.02 M PBS containing 3% BSA. Examination was done under a Zeiss LSM 510 microscope. For detection of SOD1 colocalization with cytochrome b5, pCMV b5-EGFP vector was transfected to the cells (kind gift from Dr. Otera and Prof. Mihara; [49]). The GFP signal was enhanced by anti-GFP antibody staining (1:100). In order to determine the localization of SOD1 in living cells, SK-N-SH cells expressing wt and L84V SOD1 were transfected with a pcDNA3.1-GFP-tagged wt and L84V SOD1 plasmid, respectively. After treatment with tunicamycin for 24 hr, the cells were further incubated with Mito-tracker or Lyso-tracker (Molecular Probes) for 30 min to visualize the mitochondria or lysosomes, respectively. Then the cells were rinsed at least three times in 0.1 M PBS and fixed with Zamboni's solution for examination under a LSM 510 confocal microscope (Zeiss, Osaka, Japan).

Electron microscopy

SK-N-SH cells stably expressing L84V SOD1 were exposed to 1 μg/ml tunicamycin for 24 h and then fixed at room temperature (RT) for 1 h in 0.1 M phosphate buffer (PB) containing 2.5% glutaraldehyde (GA) and 2% paraformaldehyde. Subsequently, the cells were post-fixed in 1% OsO_4 at RT for 1 h, dehydrated in a graded ethanol series, and embedded in epoxy resin (Quetol 812; Nisshin EM Co.). Areas containing cells with aggregates were block-mounted in epoxy resin by the direct epoxy-resin embedding method and cut into 90-nm sections. The sections were counterstained with uranyl acetate and lead citrate, and then examined using an H-7100 electron microscope (Hitachi).

Immune Electron microscopy

As with immunocytocemistry methods above, after fixation with Zamboni solution containing 0.1% GA, the cells with anti-SOD1 antibody were developed with DAB. Then, they were post-fixed in 1% OsO4 in 0.1 M PB at RT for 30 min after 1% GA in 0.1M PB re-fixation. The samples were dehydrated in a graded ethanol series and then embedded in Quetol 812. Areas containing cells with aggregate morphology were block-mounted and cut into 90-nm sections. The sections were counterstained with uranyl acetate and lead citrate, and then examined with an H-7100 electron microscope.

Analysis of inclusion bodies (light microscopy and electron microscopy)

Sections of SK-N-SH cells containing eosinophilic hyaline inclusion bodies and spinal cord sections from transgenic SOD1 L84V mice were decolorized, rehydrated, rinsed in 0.1 M PBS, and then blocked for 1 h in 0.1 M PBS containing 0.3% Triton X-100 and 3% BSA. Next, the sections were incubated overnight at 4°C with the primary antibody (polyclonal sheep anti-SOD1 antibody at 1:500) in 0.1 M PBS containing 0.3% Triton X-100 and 3% BSA. After washing in 0.1 M PBS, sections were incubated for 30 min with the secondary antibody (biotinylated anti-sheep IgG). Subsequently, incubation was performed for 30 min in 3% H_2O_2 to eliminate endogenous peroxidases. After amplification with avidin-biotin complex (ABC kit, Vector Laboratories), visualization of reaction products was done with 0.05 M TBS (pH 7.6) containing 1.25% DAB and 0.75% hydrogen peroxide.

For electron microscopy, samples of SK-N-SH cells expressing L84V SOD1 and spinal cords from transgenic SOD1 L84V mice were decolorized, rehydrated, and rinsed in 0.1 M PBS. The samples were further fixed and dehydrated. Then the samples were embedded directly in epoxy resin, sectioned, counterstained, and examined as described under electron microscopy section.

SUPPORTING INFORMATION

Figure S1 Cytosolic localization of SOD1 in wt SOD1 expressing cells under ER stress. (A-F, A′-F′) Analysis of localization of SOD1 on ER. WT SOD1-expressing SK-N-SH cells were incubated for 24 h without (A-F) or with 1 ug/ml of tunicamycin (A′-F′). Then the cells were fixed and stained using an anti-SOD1 antibody (green; A, D, A′, D′) and an anti-KDEL antibody (red; B, B′) or an anti-GRP78 antibody (red; E, E′). GFP-cytochrome b5 were transfected to the cells and stained with anti-GFP (green; G, G′) and anti-SOD1 (red; H, H′) antibodies. Merged images (C, F, I, C′ F′, I′). (J-R, J′-R′) Analysis of SOD1 localization to the mitochondria. WT SOD1-expressing SK-N-SH cells were treated as described in above. The locations of the mitochondria and SOD1 were visualized in WT SOD1-expressing SK-N-SH cells using 100 nM Mito-tracker (red; K, K′), an anti-Tim17 antibody (red; N, N′) or an anti-Tom20 antibody (red; Q, Q′) and an anti-SOD1 antibody (green; J, M, P, J′, M′, P′). Merged images (L, O, R, L′, O′, R′). (S-U, S′-U′) Investigation of SOD1 localization to the Golgi apparatus. L84V SOD1-expressing SK-N-SH cells were treated as described in above. Then the cells were stained with anti-SOD1 antibody (green; S, S′) and anti-GM130 antibody (red; T, T′). Merged images (U, U′). (V-X, V′-X′) Analysis of the localization of SOD1 to the lysosomes. A GFP-tagged WT SOD1 vector was transfected into WT SOD1-expressing SK-N-SH cells. After 24 h of incubation with 1 ug/ml of tunicamycin, the cells were incubated for a further 30 min with 100 nM Lyso-tracker (red; W, W′) to visualize the lysosomes. GFP channel (V, V′) Merged images (X, X′). Scale bars = 20 um.
Found at: doi:10.1371/journal.pone.0001030.s001 (3.70 MB TIF)

ACKNOWLEDGMENTS

We are grateful to Dr. Otera and Prof. Mihara (Kyusyu University, Graduate School of Medical Science) and Dr. J. Niwa and Prof. G. Sobue (Nagoya University, Graduate School of Medicine) for providing anti-Tim17 and anti-Tom20 antibodies and myc-tagged ubiquitin expression vector, respectively. We thank Dr. K. Oono, Dr. S. Matsuda and Dr. T. Kudo (Osaka University, Graduate School of Medicine) for discussion and valuable advice. We thank Dr. George Wilkinson (Max-Planck Institute of Neurobiology) for critically reading the manuscript.

Author Contributions

Conceived and designed the experiments: SY YK TK SK MT. Performed the experiments: SY YK TK MT. Analyzed the data: SY YK TK MT JH MK MA YI SK MT. Contributed reagents/materials/analysis tools: SY YK TK MK MA YI. Wrote the paper: SY YK TK SK MT.

REFERENCES

1. Gurney ME (2000) What transgenic mice tell us about neurodegenerative disease. Bioessays 22: 297–304.
2. Brown RH Jr., Robberecht W (2001) Amyotrophic lateral sclerosis: pathogenesis. Semin Neurol 21: 131–139.
3. Cleveland DW, Rothstein JD (2001) From Charcot to Lou Gehrig: deciphering selective motor neuron death in ALS. Nat Rev Neurosci 2: 806–819.
4. Rowland LP, Shneider NA (2001) Amyotrophic lateral sclerosis. N Engl J Med 344: 1688–1700.
5. Julien JP (2001) Amyotrophic lateral sclerosis. unfolding the toxicity of the misfolded. Cell 104: 581–591.
6. Bruijn LI, Miller TM, Cleveland DW (2004) Unraveling the mechanisms involved in motor neuron degeneration in ALS. Annu Rev Neurosci 27: 723–749.
7. Rosen DR, Siddique T, Patterson D, Figlewicz DA, Sapp P, et al. (1993) Mutations in Cu/Zn superoxide dismutase gene are associated with familial amyotrophic lateral sclerosis. Nature 362: 59–62.
8. Forman MS, Lee VM, Trojanowski JQ (2003) 'Unfolding' pathways in neurodegenerative disease. Trends Neurosci 26: 407–410.
9. Kaufman RJ (2002) Orchestrating the unfolded protein response in health and disease. J Clin Invest 110: 1389–1398.
10. Tirasophon W, Welihinda AA, Kaufman RJ (1998) A stress response pathway from the endoplasmic reticulum to the nucleus requires a novel bifunctional protein kinase/endoribonuclease (Ire1p) in mammalian cells. Genes Dev 12: 1812–1824.
11. Wang B, Nguyen M, Breckenridge DG, Stojanovic M, Clemons PA, et al. (2003) Uncleaved BAP31 in association with A4 protein at the endoplasmic reticulum is an inhibitor of Fas-initiated release of cytochrome c from mitochondria. J Biol Chem 278: 14461–14468.
12. Bonifacino JS, Weissman AM (1998) Ubiquitin and the control of protein fate in the secretory and endocytic pathways. Annu Rev Cell Dev Biol 14: 19–57.
13. Travers KJ, Patil CK, Wodicka L, Lockhart DJ, Weissman JS, et al. (2000) Functional and genomic analyses reveal an essential coordination between the unfolded protein response and ER-associated degradation. Cell 101: 249–258.
14. Urano F, Wang X, Bertolotti A, Zhang Y, Chung P, et al. (2000) Coupling of stress in the ER to activation of JNK protein kinases by transmembrane protein kinase IRE1. Science 287: 664–666.
15. Nakagawa T, Yuan J (2000) Cross-talk between two cysteine protease families. Activation of caspase-12 by calpain in apoptosis. J Cell Biol 150: 887–894.
16. Nakagawa T, Zhu H, Morishima N, Li E, Xu J, et al. (2000) Caspase-12 mediates endoplasmic-reticulum-specific apoptosis and cytotoxicity by amyloid-beta. Nature 403: 98–103.
17. Katayama T, Imaizumi K, Sato N, Miyoshi K, Kudo T, et al. (1999) Presenilin-1 mutations downregulate the signalling pathway of the unfolded-protein response. Nat Cell Biol 1: 479–485.
18. Katayama T, Imaizumi K, Honda A, Yoneda T, Kudo T, et al. (2001) Disturbed activation of endoplasmic reticulum stress transducers by familial Alzheimer's disease-linked presenilin-1 mutations. J Biol Chem 276: 43446–43454.

19. Dickson KM, Bergeron JJ, Shames I, Colby J, Nguyen DT, et al. (2002) Association of calnexin with mutant peripheral myelin protein-22 ex vivo: a basis for "gain-of-function" ER diseases. Proc Natl Acad Sci U S A 99: 9852–9857.
20. Nishitoh H, Matsuzawa A, Tobiume K, Saegusa K, Takeda K, et al. (2002) ASK1 is essential for endoplasmic reticulum stress-induced neuronal cell death triggered by expanded polyglutamine repeats. Genes Dev 16: 1345–1355.
21. Takahashi R, Imai Y (2003) Pael receptor, endoplasmic reticulum stress, and Parkinson's disease. J Neurol 250 Suppl 3: III25–29.
22. Takahashi R, Imai Y, Hattori N, Mizuno Y (2003) Parkin and endoplasmic reticulum stress. Ann N Y Acad Sci 991: 101–106.
23. Hitomi J, Katayama T, Eguchi Y, Kudo T, Taniguchi M, et al. (2004) Involvement of caspase-4 in endoplasmic reticulum stress-induced apoptosis and Abeta-induced cell death. J Cell Biol 165: 347–356.
24. Kato S, Takikawa M, Nakashima K, Hirano A, Cleveland DW, et al. (2000) New consensus research on neuropathological aspects of familial amyotrophic lateral sclerosis with superoxide dismutase 1 (SOD1) gene mutations: inclusions containing SOD1 in neurons and astrocytes. Amyotroph Lateral Scler Other Motor Neuron Disord 1: 163–184.
25. Kato S, Horiuchi S, Liu J, Cleveland DW, Shibata N, et al. (2000) Advanced glycation endproduct-modified superoxide dismutase-1 (SOD1)-positive inclusions are common to familial amyotrophic lateral sclerosis patients with SOD1 gene mutations and transgenic mice expressing human SOD1 with a G85R mutation. Acta Neuropathol (Berl) 100: 490–505.
26. Kato S, Saito M, Hirano A, Ohama E (1999) Recent advances in research on neuropathological aspects of familial amyotrophic lateral sclerosis with superoxide dismutase 1 gene mutations: neuronal Lewy body-like hyaline inclusions and astrocytic hyaline inclusions. Histol Histopathol 14: 973–989.
27. Hirano A, Kurland LT, Sayre GP (1967) Familial amyotrophic lateral sclerosis. A subgroup characterized by posterior and spinocerebellar tract involvement and hyaline inclusions in the anterior horn cells. Arch Neurol 16: 232–243.
28. Wate R, Ito H, Zhang JH, Ohnishi S, Nakano S, et al. (2005) Expression of an endoplasmic reticulum-resident chaperone, glucose-regulated stress protein 78, in the spinal cord of a mouse model of amyotrophic lateral sclerosis. Acta Neuropathol (Berl) 110: 557–562.
29. Aoki M, Abe K, Houi K, Ogasawara M, Matsubara Y, et al. (1995) Variance of age at onset in a Japanese family with amyotrophic lateral sclerosis associated with a novel Cu/Zn superoxide dismutase mutation. Ann Neurol 37: 676–679.
30. Shibata N, Hirano A, Kobayashi M, Siddique T, Deng HX, et al. (1996) Intense superoxide dismutase-1 immunoreactivity in intracytoplasmic hyaline inclusions of familial amyotrophic lateral sclerosis with posterior column involvement. J Neuropathol Exp Neurol 55: 481–490.
31. Bruijn LI, Becher MW, Lee MK, Anderson KL, Jenkins NA, et al. (1997) ALS-linked SOD1 mutant G85R mediates damage to astrocytes and promotes rapidly progressive disease with SOD1-containing inclusions. Neuron 18: 327–338.
32. Niwa J, Ishigaki S, Hishikawa N, Yamamoto M, Doyu M, et al. (2002) Dorfin ubiquitylates mutant SOD1 and prevents mutant SOD1-mediated neurotoxicity. J Biol Chem 277: 36793–36798.
33. Urushitani M, Kurisu J, Tateno M, Hatakeyama S, Nakayama K, et al. (2004) CHIP promotes proteasomal degradation of familial ALS-linked mutant SOD1 by ubiquitinating Hsp/Hsc70. J Neurochem 90: 231–244.
34. Higgins CM, Jung C, Ding H, Xu Z (2002) Mutant Cu, Zn superoxide dismutase that causes motoneuron degeneration is present in mitochondria in the CNS. J Neurosci 22: RC215.
35. Tobisawa S, Hozumi Y, Arawaka S, Koyama S, Wada M, et al. (2003) Mutant SOD1 linked to familial amyotrophic lateral sclerosis, but not wild-type SOD1, induces ER stress in COS7 cells and transgenic mice. Biochem Biophys Res Commun 303: 496–503.
36. Kikuchi H, Almer G, Yamashita S, Guegan C, Nagai M, et al. (2006) Spinal cord endoplasmic reticulum stress associated with a microsomal accumulation of mutant superoxide dismutase-1 in an ALS model. Proc Natl Acad Sci U S A 103: 6025–6030.
37. Sasaki S, Warita H, Abe K, Iwata M (2005) Impairment of axonal transport in the axon hillock and the initial segment of anterior horn neurons in transgenic mice with a G93A mutant SOD1 gene. Acta Neuropathol (Berl) 110: 48–56.
38. Kato S, Nakashima K, Horiuchi S, Nagai R, Cleveland DW, et al. (2001) Formation of advanced glycation end-product-modified superoxide dismutase-1 (SOD1) is one of the mechanisms responsible for inclusions common to familial amyotrophic lateral sclerosis patients with SOD1 gene mutation, and transgenic mice expressing human SOD1 gene mutation. Neuropathology 21: 67–81.
39. Taylor JP, Hardy J, Fischbeck KH (2002) Toxic proteins in neurodegenerative disease. Science 296: 1991–1995.
40. Hyun DH, Lee M, Halliwell B, Jenner P (2003) Proteasomal inhibition causes the formation of protein aggregates containing a wide range of proteins, including nitrated proteins. J Neurochem 86: 363–373.
41. Kato S, Horiuchi S, Nakashima K, Hirano A, Shibata N, et al. (1999) Astrocytic hyaline inclusions contain advanced glycation endproducts in familial amyotrophic lateral sclerosis with superoxide dismutase 1 gene mutation: immunohistochemical and immunoelectron microscopical analyses. Acta Neuropathol (Berl) 97: 260–266.
42. Kato S, Sumi-Akamaru H, Fujimura H, Sakoda S, Kato M, et al. (2001) Copper chaperone for superoxide dismutase co-aggregates with superoxide dismutase 1 (SOD1) in neuronal Lewy body-like hyaline inclusions: an immunohistochemical study on familial amyotrophic lateral sclerosis with SOD1 gene mutation. Acta Neuropathol (Berl) 102: 233–238.
43. Kato S, Saeki Y, Aoki M, Nagai M, Ishigaki A, et al. (2004) Histological evidence of redox system breakdown caused by superoxide dismutase 1 (SOD1) aggregation is common to SOD1-mutated motor neurons in humans and animal models. Acta Neuropathol (Berl) 107: 149–158.
44. Bassik MC, Scorrano L, Oakes SA, Pozzan T, Korsmeyer SJ (2004) Phosphorylation of BCL-2 regulates ER Ca(2+) homeostasis and apoptosis. Embo J 23: 1207–1216.
45. Wootz H, Hansson I, Korhonen L, Lindholm D (2006) XIAP decreases caspase-12 cleavage and calpain activity in spinal cord of ALS transgenic mice. Exp Cell Res 312: 1890–1898.
46. Wootz H, Hansson I, Korhonen L, Napankangas U, Lindholm D (2004) Caspase-12 cleavage and increased oxidative stress during motoneuron degeneration in transgenic mouse model of ALS. Biochem Biophys Res Commun 322: 281–286.
47. Ishihara N, Mihara K (1998) Identification of the protein import components of the rat mitochondrial inner membrane, rTIM17, rTIM23, and rTIM44. J Biochem (Tokyo) 123: 722–732.
48. Kanaji S, Iwahashi J, Kida Y, Sakaguchi M, Mihara K (2000) Characterization of the signal that directs Tom20 to the mitochondrial outer membrane. J Cell Biol 151: 277–288.
49. Kato H, Sakaki K, Mihara K (2006) Ubiquitin-proteasome-dependent degradation of mammalian ER stearoyl-CoA desaturase. J Cell Sci 119: 2342–2353.

Acta Neuropathol (2005) 110: 101–112
DOI 10.1007/s00401-005-1019-3

REGULAR PAPER

Shinsuke Kato · Masako Kato · Yasuko Abe
Tomohiro Matsumura · Takeshi Nishino · Masashi Aoki
Yasuto Itoyama · Kohtaro Asayama · Akira Awaya
Asao Hirano · Eisaku Ohama

Redox system expression in the motor neurons in amyotrophic lateral sclerosis (ALS): immunohistochemical studies on sporadic ALS, superoxide dismutase 1 (SOD1)-mutated familial ALS, and SOD1-mutated ALS animal models

Received: 21 September 2004 / Revised: 9 March 2005 / Accepted: 9 March 2005 / Published online: 28 June 2005

Abstract Peroxiredoxin-II (PrxII) and glutathione peroxidase-1 (GPx1) are regulators of the redox system that is one of the most crucial supporting systems in neurons. This system is an antioxidant enzyme defense system and is synchronously linked to other important cell supporting systems. To clarify the common self-survival mechanism of the residual motor neurons affected by amyotrophic lateral sclerosis (ALS), we examined motor neurons from 40 patients with sporadic ALS (SALS) and 5 patients with superoxide dismutase 1 (SOD1)-mutated familial ALS (FALS) from two different families (frameshift 126 mutation and A4 V) as well as four different strains of the SOD1-mutated ALS models (H46R/G93A rats and G1H/G1L-G93A mice). We investigated the immunohistochemical expression of PrxII/GPx1 in motor neurons from the viewpoint of the redox system. In normal subjects, PrxII/GPx1 immunoreactivity in the anterior horns of the normal spinal cords of humans, rats and mice was primarily identified in the neurons: cytoplasmic staining was observed in almost all of the motor neurons. Histologically, the number of spinal motor neurons in ALS decreased with disease progression. Immunohistochemically, the number of neurons negative for PrxII/GPx1 increased with ALS disease progression. Some residual motor neurons coexpressing PrxII/GPx1 were, however, observed throughout the clinical courses in some cases of SALS patients, SOD1-mutated FALS patients, and ALS animal models. In particular, motor neurons overexpressing PrxII/GPx1, i.e., neurons showing redox system up-regulation, were commonly evident during the clinical courses in ALS. For patients with SALS, motor neurons overexpressing PrxII/GPx1 were present mainly within approximately 3 years after disease onset, and these overexpressing neurons thereafter decreased in number dramatically as the disease progressed. For SOD1-mutated FALS patients, like in SALS patients, certain residual motor neurons without inclusions also overexpressed PrxII/GPx1 in the short-term-surviving FALS patients. In the ALS animal models, as in the human diseases, certain residual motor neurons showed overexpression of PrxII/GPx1 during their clinical courses. At the terminal stage of ALS, however, a disruption of this common PrxII/GPx1-overexpression mechanism in neurons was observed. These findings lead us to the conclusion that the residual ALS neurons showing redox system up-regulation would be less susceptible to ALS stress and protect themselves from ALS neuronal death, whereas the breakdown of this redox system at the advanced disease stage accelerates neuronal degeneration and/or the process of neuronal death.

S. Kato (✉) · E. Ohama
Department of Neuropathology, Institute of Neurological Sciences, Faculty of Medicine, Tottori University, Nishi-cho 36-1, 683-8504 Yonago, Japan
E-mail: kato@grape.med.tottori-u.ac.jp
Tel.: +81-859-348034
Fax: +81-859-348289

M. Kato
Division of Pathology, Tottori University Hospital, Yonago, Japan

Y. Abe · T. Matsumura · T. Nishino
Department of Biochemistry and Molecular Biology, Nippon Medical School, Tokyo, Japan

M. Aoki · Y. Itoyama
Department of Neuroscience, Division of Neurology, Tohoku University Graduate School of Medicine, Sendai, Japan

K. Asayama
Department of Pediatrics, University of Occupational and Environmental Health, Kitakyushu, Japan

A. Awaya
Japan Science and Technology Agency, Tachikawa, Japan

A. Hirano
Division of Neuropathology, Department of Pathology, Montefiore Medical Center, Bronx, New York, USA

Keywords Amyotrophic lateral sclerosis · Peroxiredoxin-II · Glutathione peroxidase-1 · Redox system

Introduction

Amyotrophic lateral sclerosis (ALS), first described by Charcot and Joffroy in 1869 [11], is a fatal and age-associated neurodegenerative disorder that primarily involves both the upper and lower motor neurons [23]. This disease has been recognized as a distinct clinicopathological entity of unknown etiology for over 130 years.

During physiological processes and in response to external stimuli such as ultraviolet radiation, cells produce reactive oxygen species (ROSs). To protect itself from these potentially destructive ROSs, each cell of the living organs has developed a sophisticated antioxidant system. In such systems, there are two groups of the enzymes: those constituting the first group convert superoxide radicals into hydrogen peroxide (H_2O_2), and those of the second convert H_2O_2 into harmless water and oxygen. The neuronal cytoplasmic isoform of the first enzyme group is superoxide dismutase 1 (SOD1) [13]. In the second enzyme group, there are the peroxiredoxin (Prx) and glutathione peroxidase (GPx) families, as well as catalase localized within peroxisomes. Unlike in SOD1 and catalase, enzymes of the Prx and GPx families require secondary enzymes and cofactors to function at high efficiency [7]. The enzymes of the Prx and GPx families are considered to play important roles in the direct control of the redox system. In general, the redox system regulates versatile control mechanisms in signal transduction and gene expression [35]. In mammalian cells, this redox signal transduction is synchronously linked to important systems such as cellular differentiation, immune response, growth control, apoptosis, and tumor growth [4, 9, 19, 26, 31, 34]. In the mammalian central nervous system (CNS), the members of Prx and GPx families regulating the neuronal cytoplasmic redox system are PrxII and GPxI, which directly control the redox system in neurons [6, 7, 8, 12, 17, 24, 27, 29, 30]. In the in vivo milieu where mutant SOD1 exists, PrxII/GPxI co-aggregates with SOD1 as neuronal Lewy body-like hyaline inclusions (LBHIs): neuronal LBHIs immunohistochemically positive for three proteins of SOD1, PrxII and GPxI are observed in the mutant SOD1-related familial ALS (FALS) patients and transgenic rats expressing human SOD1 with H46R and G93A mutations [24]. Although some motor neurons with SOD1 gene mutation form inclusions that are positive for these three proteins, other SOD1-mutated motor neurons progress to cell death without forming the inclusions.

On the other hand, an essential histopathological feature of ALS is loss of the large anterior horn cells throughout the spinal cord, with the surviving motor neurons of the spinal cord exhibiting shrinkage. Among these residual large anterior horn cells, some appear to be normal. These surviving motor neurons in ALS patients are thought to possess some form of self-preservation mechanism. To gain new insight into the survival mechanism of these residual motor neurons, we focused on the redox system. In the study presented here, we performed immunohistochemical analyses of the spinal cord, not only from FALS patients with SOD1 gene mutations and SOD1-mutated ALS animal models, but also from patients with sporadic ALS (SALS), and analyzed the expression of PrxII/GPxI (redox system) in the residual motor neurons.

Materials and methods

Autopsy specimens

Histochemical and immunohistochemical studies were performed on archival, buffered 10% formalin-fixed, paraffin-embedded spinal cord tissues obtained at autopsy from 40 SALS patients and 5 FALS patients, who were members of two different families. The main clinical characteristics of the SALS patients are summarized in Fig. 2. The clinicopathological characteristics of the FALS patients are summarized in Table 1 and have been reported previously [20, 21, 25, 28, 33, 36, 38]. SOD1 analysis revealed that the members of the Japanese Oki family had a two-base pair deletion at codon 126 (frameshift 126 mutation) [20] and that the members of the American C family had an Ala to Val substitution at codon 4 (A4V) [36]. As controls for human samples, we examined autopsy specimens of the spinal cord from 20 neurologically and neuropatho-

Table 1 Characteristics of five FALS cases (*FALS* familial amyotrophic lateral sclerosis, *SOD* superoxide dismutase, *LBHI* Lewy body-like hyaline inclusion, *2-bp* two-base pair, *PCI* posterior column involvement type, + detected, *ND* not determined, *As* asphyxia, *IH* intraperitoneal hemorrhage, *RD* respiratory distress, *Pn* pneumonia)

Case	Age	Sex	Cause of death	FALS duration	SOD1 mutation	FALS subtype	Neuronal LBHI
Japanese Oki family							
1	46	F	As	18 months	2-bp deletion (126)	PCI	+
2	65	M	IH	11 years	2-bp deletion (126)	PCI and degeneration of other systems	+
American C family							
3	39	M	RD	7 months	A4V	PCI	+
4	46	M	Pn	8 months	A4V	PCI	+
5	66	M	Pn	1 year	ND	PCI	+

logically normal individuals (11 males, 9 females; aged 37–75 years).

Animal models

Histochemical and immunohistochemical studies were also carried out on specimens from ALS animal models: transgenic rats and mice carrying the overexpressed human mutant SOD1 genes. The H46R rats used in this study were a transgenic line (H46R-4) in which the level of human SOD1 with the H46R mutation was 6 times the level of endogenous rat SOD1 [32]. The G93A rats were a transgenic line (G93A-39) in which the level of human SOD1 with the G93A mutation was 2.5 times the level of endogenous rat SOD1 [32]. The G93A mice used in this study represented two lines of transgenic mice carrying the overexpressed human G93A mutant SOD1 gene: high copy G93A mice [B6SJL-TgN(SOD1-G93A)1Gur, JR2726; G1H-G93A] and low copy G93A mice [B6SJL-TgN(SOD1-G93A)1Gur^{dl}, JR2300; G1L-G93A] (Jackson Laboratory, Bar Harbor, ME). The H46R rats were killed at 110 ($n=1$), 135 ($n=1$), 160 ($n=1$), 170 ($n=1$), and over 180 ($n=3$) days after birth. The G93A rats were killed at 70 ($n=1$), 90 ($n=1$), 110 ($n=1$), 130 ($n=1$), 150 ($n=1$), and over 180 ($n=3$) days after birth. The detailed clinical signs and pathological characteristics of the H46R and G93A rats have been demonstrated previously [32]. As rat controls, we investigated the spinal cord specimens of each of eight age-matched littermates of the H46R and G93A rats. The G1H-G93A mice were examined at 90 ($n=2$), 100 ($n=2$), 110 ($n=3$), and 120 ($n=3$) days of age. The G1L-G93A mice were examined at 90 ($n=1$), 100 ($n=1$), 120 ($n=1$), 150 ($n=1$), 180 ($n=1$), 190 ($n=1$), 215 ($n=1$), 230 ($n=1$), and over 250 ($n=2$) days of age. As mouse controls, we also examined the spinal cord specimens of each of ten age-matched littermates of the G1H-G93A and G1L-G93A mice. Rats and mice were anesthetized with sodium pentobarbital (0.1 ml/100 g body weight). After perfusion of the animals via the aorta with physiological saline at 37°C, they were fixed by perfusion with 4% paraformaldehyde in 0.1 M cacodylate buffer (pH 7.3). The spinal cords were removed and then postfixed in the same solution. This study was approved by the Institutional Animal Care and Use Committee of Tottori University (Permission no. 03-S-18).

Histochemistry and immunohistochemistry

After fixation, the specimens were embedded in paraffin, cut into 6-μm-thick sections and examined by light microscopy. Spinal cord sections were stained by the following histochemical methods: hematoxylin and eosin (HE), Klüver-Barrera, Holzer, phosphotungstic acid-hematoxylin, periodic acid-Schiff, alcian blue, Masson's trichrome, Mallory azan, and Gallyas-Braak stains.

Rat PrxII, which contained a 6-His-tagged sequence at the N-terminal region, was overexpressed using *Escherichia coli* strain BL21 (DE3) cells harboring the expression plasmid pET30a (Novagen, Darmstadt, Germany) -PrxII, according to the modified method by Hirotsu et al. [15]. The His-tagged PrxII induced with 0.1 mM isopropyl-β-D-thiogalactoside (IPTG) was purified by a Ni^{2+}-nitrilotriacetate column (Qiagen, Hilden, Germany) and then digested with enterokinase. Finally, the purified PrxII was passed through an Erapture Agarose column for removal of enterokinase (Novagen). The PrxII gene was prepared from a rat liver cDNA library (Takara Biomedicals, Otsu, Japan) by PCR using the primers, 5'-TTCCATGGCCTCCGG-CAACGCGCACAT-3' and 5'-TTGGATCCATCTCA-GTTGTGTTTGGAG-3'. Utilizing this purified recombinant rat Prxll protein (amino acids 1–198), we produced a rabbit polyclonal antibody against rat PrxII according to the method previously described by Kato et al. [24].

Representative paraffin sections were used for immunohistochemical assays. The following primary antibodies were used: a rabbit polyclonal antibody against rat Prxll (amino acids 1–198) [diluted 1:2,000 in 1% bovine serum albumin-containing phosphate-buffered saline (BSA-PBS), pH 7.4]; an affinity-purified rabbit antibody against a synthetic peptide corresponding to the C-terminal region of Prxll (amino acids 184–198; this amino acid sequence is homologous with those of the C-terminal regions of the human, rat or mouse Prxll.) (concentration: 1 μg/ml) [24]; a polyclonal antibody to GPxl [diluted 1:2,000 in 1% BSA-PBS, pH 7.4] [3]; a polyclonal antibody to human SOD1 (diluted 1:10,000 in 1% BSA-PBS, pH 7.4) [2]; and a monoclonal antibody to human SOD1 (concentration: 3 μg/ml; MBL, Nagoya, Japan). Sections were deparaffinized, and endogenous peroxidase activity was quenched by incubation for 30 min with 0.3% H_2O_2. The sections were then washed in PBS. Normal sera homologous with the secondary antibodies were used as a blocking reagent. Tissue sections were incubated with the primary antibodies for 18 h at 4°C. PBS-exposed sections served as controls. As a further control, some sections were incubated with the polyclonal antibody against rat Prxll that had been preabsorbed with an excess amount of the recombinant rat Prxll protein. Bound antibodies were visualized by the avidin-biotin-immunoperoxidase complex (ABC) method using the appropriate Vectastain ABC kits (Vector Laboratories, Burlingame, CA) and 3,3'-diaminobenzidine tetrahydrochloride (DAB; Dako, Glostrup, Denmark) as chromogen.

Western blot analysis

This analysis was carried out on three fresh autopsy specimens from spinal cord cervical segments obtained from two SALS cases [2.5 years after onset (case 19 in Fig. 2: age 63 years) and 11 years 5 months after onset

(case 40 in Fig. 2: age 51 years)] and one normal individual (age 68 years). In brief, specimens were homogenized in Laemmli sample buffer (Bio-Rad, Hercules, CA) containing 2% sodium dodecyl sulfate (SDS), 25% glycerol, 10% 2-mercaptoethanol, 0.01% bromophenol blue, and 62.5 mM TRIS-HCl (pH 6.8). The samples were heated at 100°C for 5 min. Soluble protein extracts (20 μg) from the samples were separated on SDS-polyacrylamide gels (4–20% gradient, Bio-Rad) and transferred by electroblotting to Immobilon PVDF (Millipore, Bedford, MA). After blocking with 5% nonfat milk for 30 min at room temperature, the blots were incubated overnight at 4°C with the antibodies against PrxII and GPxI. Binding to PrxII and GPxI was visualized with the Vectastain ABC Kit and DAB. Appropriate molecular weight markers (Bio-Rad) were included in each run.

Results

Histopathology

An important histopathological finding in the spinal cord in SALS was loss of motor neurons throughout the

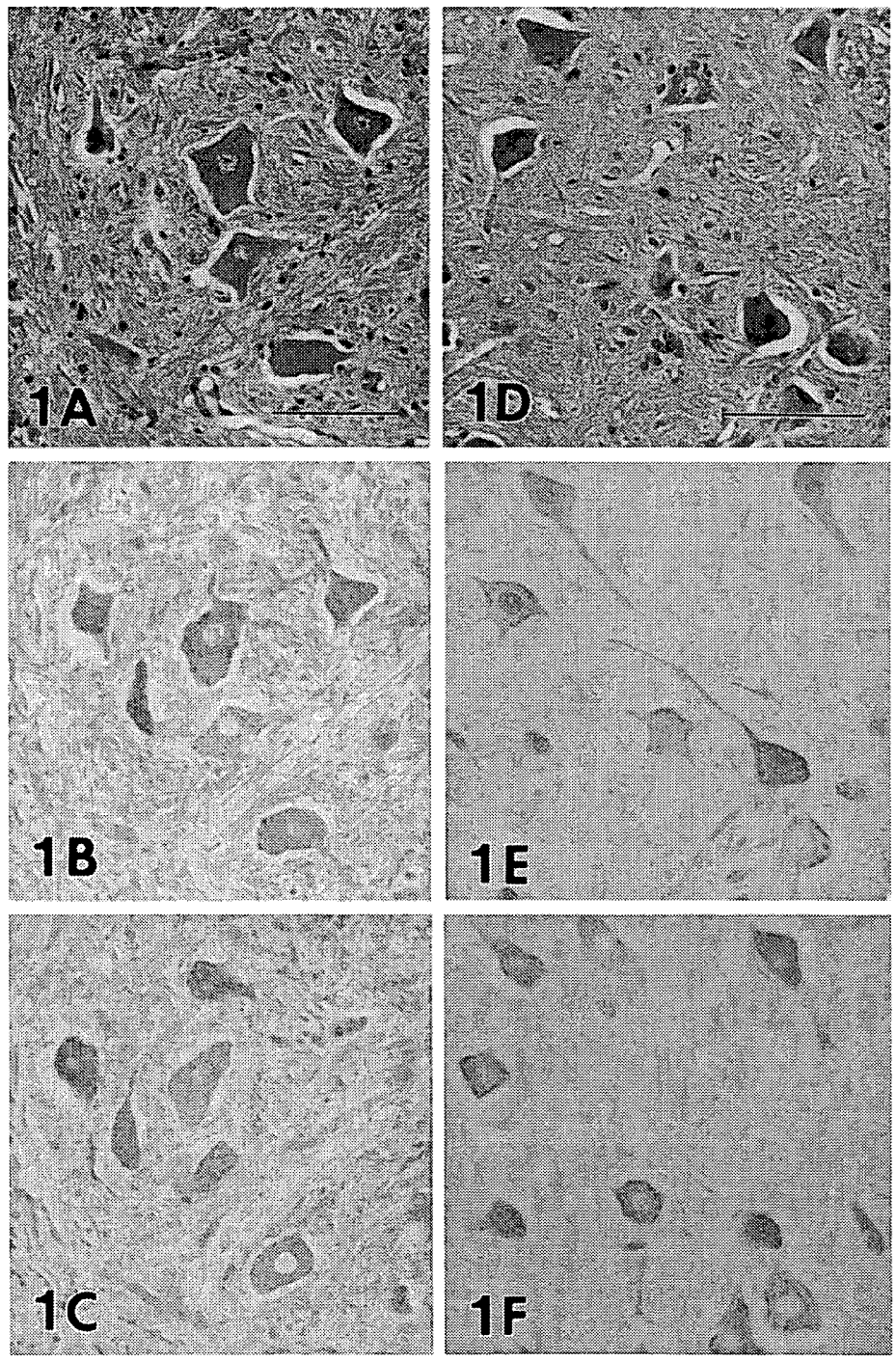

Fig. 1 Detection of PrxII and GPxI in serial sections of the normal anterior horn cells of the spinal cord in humans (**A–C**) and rats (**D–F**). **A, D** HE staining. **B, E** Immunoreactive for PrxII: immunostaining with the antibody against synthetic peptide corresponding to the C-terminal region of PrxII (**B**) and immunostaining with the antibody to rat PrxII (**E**). Immunoreactivity is identified in most of the anterior horn cells. **C, F** Immunostaining for GPxI. Almost all of the anterior horn cells in the spinal cord coexpress both PrxII (**B, E**) and GPxI (**C, F**) in comparison with HE-stained serial sections (**A, D**), although their staining intensities in neurons vary. **B, C, E, F** No counterstaining. (*HE* hematoxylin and eosin, *PrxII* peroxiredoxin-II, *GPxI* glutathione peroxidase-I). *Bars* **A** (also for **B, C**), **D** (also for **E, F**) 100 μm

course of the disease. In the specimens we examined, neuronal loss was most easily recognized in the cervical and lumbar enlargements. The surviving motor neurons showed shrinkage, and lipofuscin granule-filled neurons stood out. Among the residual motor neurons, some appeared to be normal. Bunina bodies were observed in the residual motor neurons. The number of motor neurons decreased with SALS disease progression. Reactive astrocytosis and gliosis were also observed in the affected areas. In the affected antero-lateral columns that were most pronounced in the crossed and uncrossed corticospinal tracts, there was a loss of large myelinated fibers in association with variable degrees of astrocytic gliosis. Fiber destruction was associated with the appearance of lipid-laden macrophages. Analysis of the essential changes in the five cases of SOD1-mutated FALS revealed a subtype of FALS with posterior column involvement (PCI). This subtype is characterized by degeneration of the middle root zones of the posterior column, Clarke nuclei, and the posterior spinocerebellar tracts, in addition to spinal cord motor neuron lesions. A patient who had survived for a long period, with a clinical course of 11 years (case 2 in Table 1), showed multi-system degeneration in addition to the features of FALS with PCI. Neuronal LBHIs were present in all five FALS cases with SOD1 gene mutations. The spinal cords of normal human individuals did not exhibit any distinct histopathological alterations.

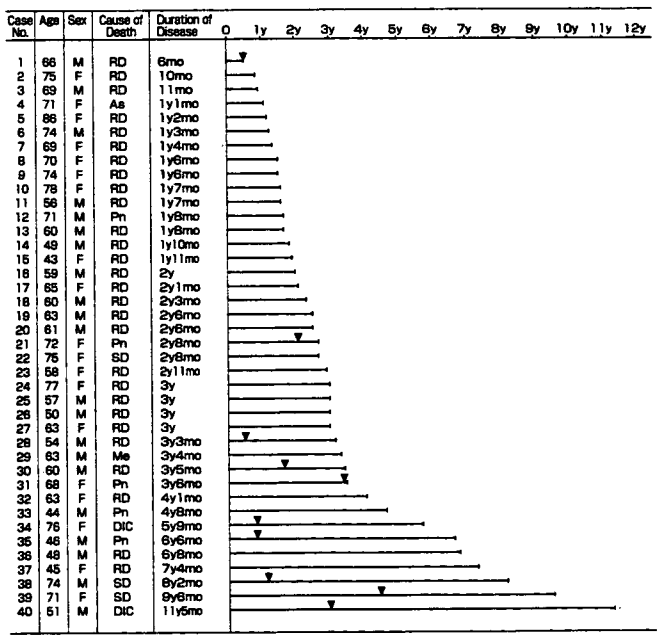

Fig. 2 Characteristics of 40 SALS cases, including patient's age, sex, cause of death, and duration of disease. The *horizontal lines* each show the duration of disease. *Arrowheads* indicate the time point at which the patients were placed on respirators (*ALS* amyotrophic lateral sclerosis, *SALS* sporadic ALS, *RD* respiratory distress, *As* asphyxia, *Pn* pneumonia, *SD* sudden death, *Me* melena, *DIC* disseminated intravascular coagulation, *y* years, *mo* months)

The clinical courses and histopathological findings of H46R and G93A transgenic rats have been reported previously by Nagai et al. [32]. As expected, the H46R rats developed motor deficits at approximately 145 days of age, and G93A rats showed the clinical signs at around 125 days of age. When we focused on the anterior horn cells, the number of the anterior horn cells of the H46R rat at 110 days of age was not significantly decreased as compared with that of the age-matched littermate. There were slightly decreased numbers of anterior horn cells with inclusions in the H46R rat at 135 days of age. At 160, 170 and over 180 days of age, the number of the anterior horn cells in the H46R rats was decreased markedly, and many inclusions including neuronal LBHIs were observed as inclusion pathology. For G93A rats, the number of the anterior horn cells at 70, 90 and 110 days of age was almost the same as that of their age-matched littermates, although at 90 and 110 days of age these rats showed vacuolation pathology including neuropil vacuoles. In G93A rats at 130, 150 and over 180 days of age, there was marked loss of the anterior horn cells, with both inclusion and vacuolation pathologies being involved. In the transgenic mice from the Jackson Laboratory, the clinical onset of the G1H-G93A mice was, as expected, about 100 days after birth, and that of G1L-G93A mice was approximately 185 days after birth. The number of the anterior horn cells of the G1H-G93A mice examined at 90 days after birth was not significantly decreased as compared with that of their age-matched littermates, whereas neuropil vacuolation was observed. The number of anterior horn cells of the G1H-G93A mice at 100 days of age was slightly decreased, and they had abundant vacuoles and a few inclusions. The G1H-G93A mice examined at 110 and 120 days of age revealed severe loss of the anterior horn cells and both inclusion and vacuolation pathologies. In the G1L-G93A mice examined at 90, 100, 120, 150 and 180 days after birth, the number of the anterior horn cells was not significantly changed compared to that of their age-matched littermates, although the G1L-G93A mice at 90, 100, 120, 150 and 180 days of age showed vacuolation pathology and, at 180 days of age, a few inclusions. In G1L-G93A mice at 190, 215, 230 and over 250 days of age, there were significant losses of anterior horn cells, with both inclusion and vacuolation pathologies being present. The spinal cords of the littermates of these animal models did not exhibit any distinct histopathological changes.

Immunohistochemistry

In the present study, we produced a rabbit polyclonal antibody against rat Prxll (amino acids 1–198), in addition to the affinity-purified rabbit antibody against a synthetic peptide corresponding to the C-terminal region of Prxll previously reported by Kato et al. [24]. This newly produced rabbit polyclonal antibody against rat Prxll was successfully applied to stain paraffin sections

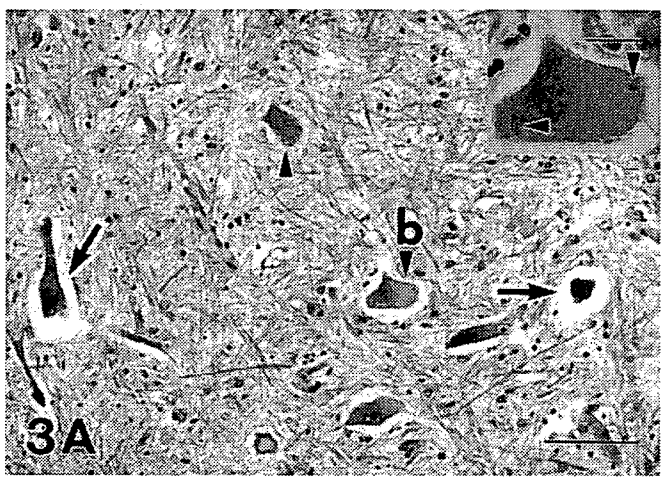

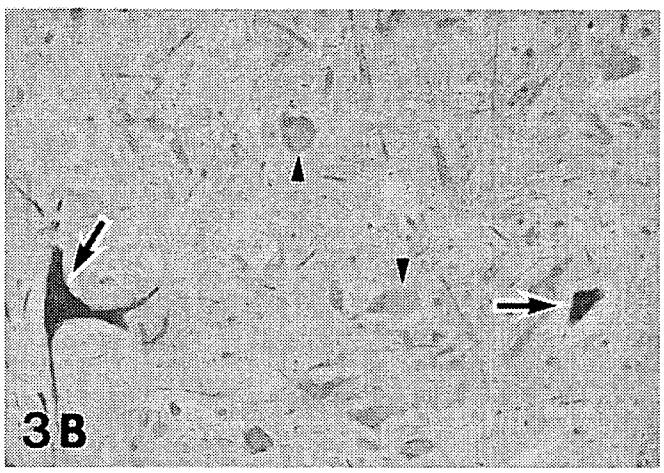

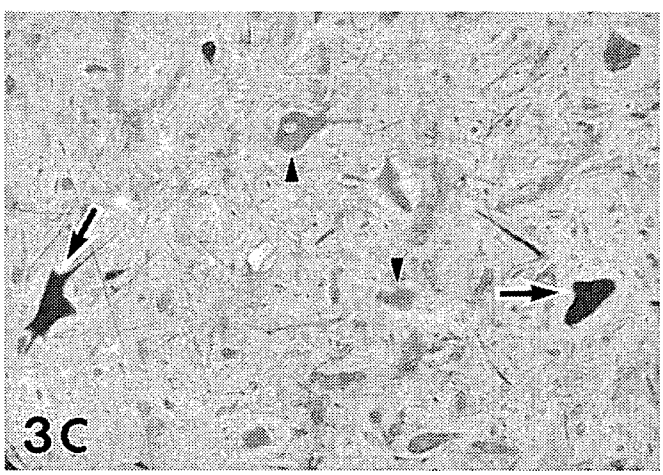

◀

Fig. 3 Serial sections of the spinal anterior horn cells in a patient with SALS after a clinical course of 2.5 years (case 19 in Fig. 2). **A** Light microscopic preparation stained with HE. *Top right inset* shows the higher magnification of a neuron (indicated by *arrowhead* with **b** in **A**), in which Bunina bodies (*arrowheads* in *top right inset*) are observed. **B** PrxII immunoreactivity of the section consecutive to that shown in **A**. **C** GPxI immunoreactivity of the section consecutive to that shown in **B**. Residual neurons overexpressing both PrxII and GPxI are evident (*arrows*). The staining pattern is diffuse in the cytoplasm and dendrites. Other neurons are either faintly stained by both antibodies, or unstained (*arrowheads*). Observation of only the HE-stained section in **A** reveals no difference between the neurons overexpressing PrxII/GPxI and those almost negative for PrxII/GPxI. No correlation is demonstrated between PrxII/GPxI expression and the presence of Bunina bodies. **B, C** No counterstaining. *Bar* **A** (also for **B, C**) 100 μm, *top right inset* in **A** 20 μm

from rats (Fig. 1E). Additionally, we were able to use this rabbit polyclonal antibody against rat Prxll to stain paraffin sections from humans and mice. Both anti-Prxll antibodies had the same ability to immunostain paraffin sections from humans, rats and mice, as well as in immunoblotting of tissue homogenate of the human spinal cord. When control and representative paraffin sections were incubated with PBS alone (i.e., no primary antibody), no staining was detected. Incubation of sections with anti-rat Prxll antibody that had been pretreated with an excess amount of the recombinant rat Prxll protein (amino acids 1–198) produced no staining in any of the sections.

As expected [24], almost all of the normal anterior horn cells in the spinal cords of humans, rats and mice coexpressed both Prxll and GPxl (Fig. 1), although their staining intensities in positively stained neurons varied. With respect to the intracellular localization of Prxll using the two anti-Prxll antibodies, immunostaining of the neuronal cytoplasm and proximal dendrites was specifically observed (Fig. 1B, E). In addition, the nuclei of some neurons were immunostained, albeit the staining intensity varied (Fig. 1E). GPxl immunostaining showed a cytoplasmic staining pattern, with the cell bodies and proximal dendrites being essentially identified (Fig. 1C, F), but no intranuclear staining was observed (Fig. 1C, F).

In SALS patients, some residual neurons expressed both Prxll and GPxl strongly within about 3 years after disease onset (cases 1–27 in Fig. 2). Other neurons were either faintly stained by both antibodies or unstained. Around 2–3 years after disease onset in SALS patients (cases 16–27 in Fig. 2), the intensity of Prxll and GPxl immunoreactivities peaked in some residual neurons that were positive for both proteins (Fig. 3). In SALS patients with a clinical course of over 3 years (cases 28–40 in Fig. 2), the number of residual neurons decreased strikingly, and respiratory assistance became essential for most patients. The residual neurons intensely expressing both Prxll and GPxl decreased with disease progression, while the number of residual neurons negative for both proteins increased dramatically (Fig. 4). At 11 years 5 months after disease onset (case 40 in Fig. 2), most of the neurons were atrophic and immunonegative for both Prxll and GPxl. However, even in this long-surviving patient, a few residual neurons expressing both Prxll and GPxl were observed (Fig. 5). Thus, residual motor neurons positive for both Prxll and GPxl were always evident throughout the disease course in every SALS patient, although after approximately 3 years of disease their number decreased dramatically. Observation of only the HE-stained sections revealed no

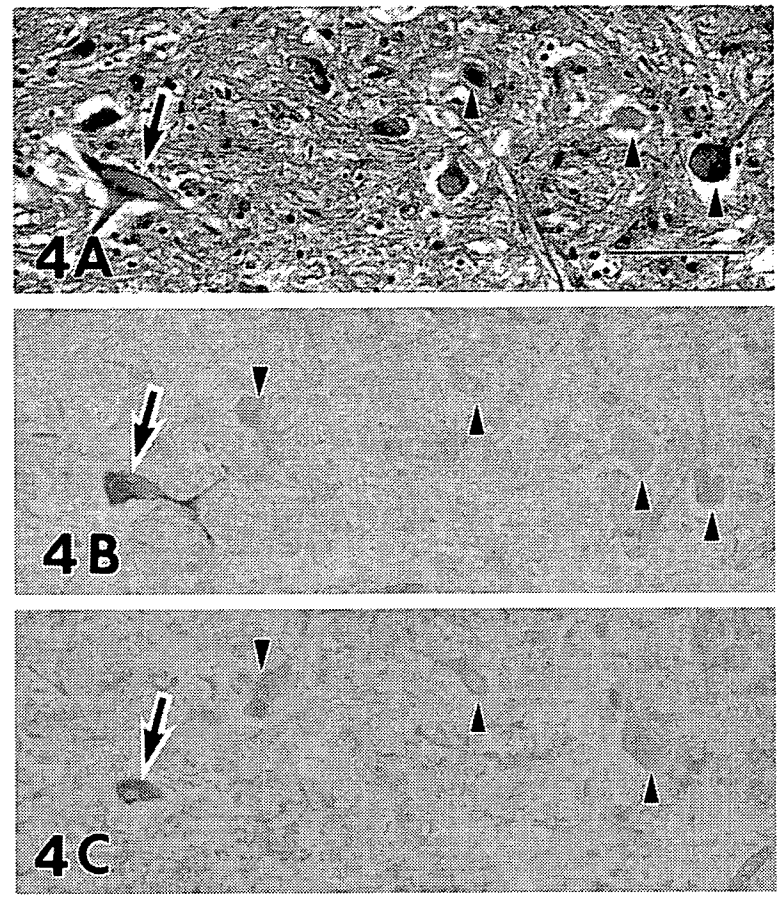

Fig. 4 Serial sections of the spinal anterior horn cells in a patient with SALS after a clinical course of 4 years 8 months (case 33). **A** In the HE preparation, residual motor neurons appear to be atrophic. There is no distinction among these atrophic neurons when observed in the HE preparation alone. **B** Immunostaining for Prxll. The number of residual neurons overexpressing Prxll (*arrow*) is reduced in comparison with that in the SALS patient after a clinical course of 2.5 years (Fig. 3). The number of Prxll-negative neurons is increased (*arrowheads*). **C** Immunostaining for GPxl. Similarly to the Prxll immunostaining, the number of GPxl-overexpressing neurons is diminished (*arrow*). In contrast, the number of GPxl-immunonegative neurons is increased (*arrowheads*). **B, C** No counterstaining. *Bar* **A** (also for **B, C**) 100 μm

difference between the neurons positive for Prxll and GPxl and those negative for both proteins (Figs. 3, 4, 5).

In the five FALS patients with SOD1 mutations, as reported previously [24], neuronal LBHIs in the anterior horn cells showed co-aggregation of Prxll/GPxl with SOD1. Although some SOD1-mutated anterior horn cells in these patients formed neuronal LBHIs, others did not. When we focused on these residual anterior horn cells without inclusions, the stainability and intensity of Prxll and GPxl staining in the residual cells without inclusions in the five FALS patients with SOD1 gene mutations were identical to those of the SALS patients. The numbers of residual anterior horn cells in one member of the Japanese Oki family (case 1, frame-shift 126 mutation in SOD1 gene) and three members of the American C family (cases 3–5, A4V substitution in the SOD1 gene), observed within 2 years of the disease onset, were similar, although the loss of the anterior horn cells in the FALS patients was generally more severe in contrast to that seen in the SALS patients with the same disease duration. As in the SALS patients within about 3 years of disease onset, some of the residual anterior horn cells with no LBHIs overexpressed Prxll/GPxl in the four short-term-surviving FALS patients from the two different families and divergent SOD1 gene mutations. In a long-term surviving patient (case 2) with a clinical course of over 10 years, there were a few residual neurons, and most were immunonegative for Prxll/GPxl. However, rare residual neurons expressing Prxll/GPxl were still evident. The findings for the long-term-surviving FALS patient with SOD1 mutation were the same as those of the long-term-surviving SALS patients.

In the ALS animal models with human mutant SOD1, the inclusions exhibited co-aggregation of Prxll/GPxl with SOD1 as reported previously [24]. Noticeably, the Prxll/GPxl-immunoreactive findings in the rat (H46R and G93A rats) and mouse (G1H-G93A and G1L-G93A mice) models were essentially the same throughout the disease course for each ALS animal model. In the preclinical stage, the Prxll/GPxl immunostainability and immunointensity of the anterior horn cells were identical to those in the anterior horn cells of the normal littermates. Although the number of the anterior horn cells in the ALS animal models was decreased after the clinical onset of disease, some of these residual anterior horn cells showed overexpression of Prxll/GPxl, i.e., up-regulation of the redox system. In particular, this redox system up-regulation in the residual motor neurons was prominent at 160 days of age in H46R rats (Fig. 6A, B), at 150 days of age in G93A rats, at 110 days of age in G1H-G93A mice (Fig. 7) and at 215 days of age in G1L-G93A mice. At the end stage of disease in the four different ALS animal models,

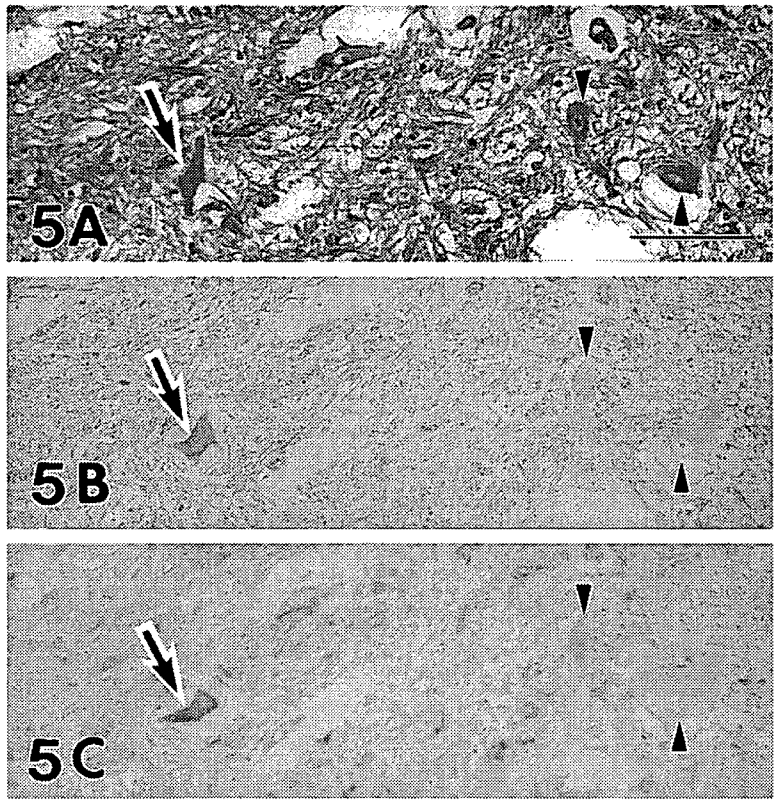

Fig. 5 Serial sections of the spinal anterior horn cells in a patient with SALS after a clinical course of 11 years 5 months (case 40). **A** Light microscopic preparation stained with HE. Small and atrophic motor neurons are seen. **B** Prxll immunoreactivity of the section consecutive to that shown in **A**. Although the residual neuron (*arrow*) appears to be atrophic in the HE preparation, this residual neuron expresses Prxll. **C** GPxl immunoreactivity of the section consecutive to that shown in **B**. The residual neuron that appears to be atrophic in the HE preparation is stained by the anti-GPxl antibody (*arrow*). Although there is no neuron overexpressing Prxll/GPxl, a neuron expressing Prxll/GPxl can be observed (*arrow*). By marked contrast, the number of neurons negative for Prxll/GPxl is increased (*arrowheads*). Observation of the HE-stained section in **A** shows no difference between the atrophic neuron positive for Prxll/GPxl (*arrow*) and the atrophic neurons negative for both proteins (*arrowheads*). **B, C** No counterstaining. *Bar* **A** (also for **B, C**) 100 μm

however, almost all of the residual motor neurons were negative for Prxll/GPxl, in marked contrast to the inclusions positive for PrxII/GPxI (Fig. 6C, D). As seen for the human specimens, no difference between the neurons positive for Prxll/GPxl and those negative for both proteins were observed the HE-stained sections for these animal models (Fig. 7).

Western blot analysis

When the tissue homogenate of each fresh cervical segment of the human spinal cord was examined by immunoblotting for Prxll, a single band corresponding to approximately 23 kDa was observed, i.e., with the same mobility as human Prxll (Fig. 8A). Immunoblotting showed that the intensity of Prxll immunoreactivity in the SALS patient with a clinical course of 2.5 years (case 19 in Fig. 2) appeared to be almost identical to that in a normal subject. In the SALS patient with a clinical course of 11 years 5 months (case 40 in Fig. 2), Prxll expression was less than that in the normal subject. This observation supported the results of Prxll immunohistochemistry. Immunoblotting for GPxl revealed a single band corresponding to about 22 kDa in two SALS cases and a normal subject (Fig. 8B). This molecular mass was compatible with that of human GPxl. In the SALS case at 2.5 years after disease onset (case 19 in Fig. 2), GPxl was expressed with almost the same intensity as that in the normal subject. However, the level of GPxl expression in the SALS case at 11 years 5 months after onset (case 40 in Fig. 2) decreased below that in the normal subject. This finding reflected the GPxl immunohistochemistry results.

Discussion

Prxll is a novel organ-specific anti-oxidative enzyme that is mainly expressed in mammalian brain [24, 29]. It is a member of the Prx family, the members of which directly regulate the redox system [6, 7, 8, 17, 29]. Prxll is a homodimeric protein composed of two subunits, each with a molecular mass of approximately 23 kDa [15, 16]. Like Prxll, GPxl, one of the major cytosolic isoforms of the GPxl family, also directly controls the redox system [12, 27, 30]. GPxl is a homotetramer consisting of approximately 22-kDa subunits [3]. This is consistent with the results of Western blot analyses, where use of

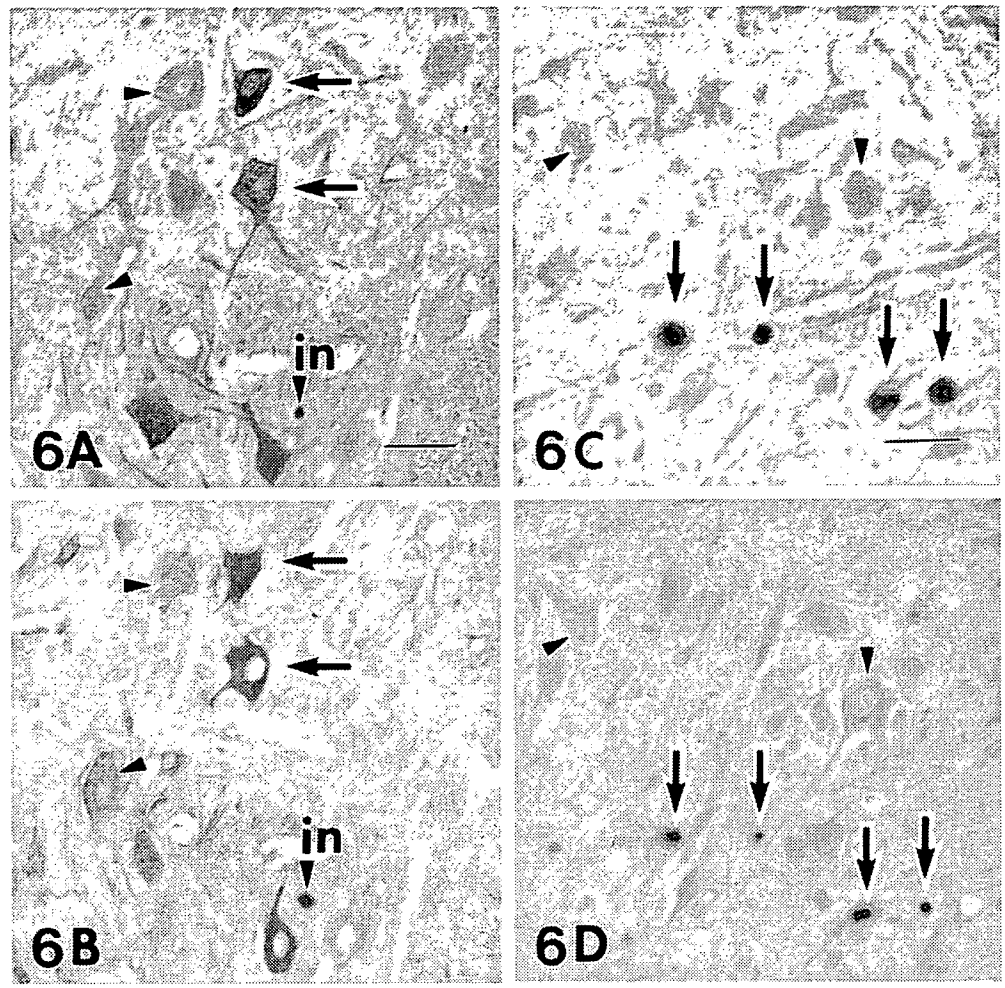

Fig. 6 Expression of Prxll and GPxl detected by immunohistochemistry in the spinal anterior horn in the transgenic rats expressing human SOD1 with an H46R mutation. **A, B** Serial sections of spinal anterior horn cells at 160 days of age in H46R rat immunostained with antibodies against Prxll (**A**) and GPxl (**B**). Residual neurons overexpressing Prxll/GPxl, i.e., showing redox system up-regulation, are observed (*arrows*). An inclusion (*arrowhead* with *in*) in the neuropil is intensely positive for Prxll/GPxl. The other neurons are either faintly stained by both antibodies, or unstained (*arrowheads*). **C, D** Serial sections of spinal anterior horn cells at over 180 days of age in H46R rat immunostained with antibodies against Prxll (**C**) and GPxl (**D**). Round and sausage-like LBHIs are strongly positive for Prxll/GPxl (*arrows*). By marked contrast, the number of neurons negative for Prxll/GPxl is increased (*arrowheads*). **A—D** No counterstaining (*SOD* superoxide dismutase, *LBHI* Lewy body-like hyaline inclusion). *Bar* **A** (also for **B**) 50 μm, **C** (also for **D**) 30 μm

the normal human tissue homogenate yielded a single band of approximately 23 kDa with the two anti-Prxll antibodies and a single band of about 22 kDa with the anti-GPxl antibody.

As expected [24], Prxll/GPxl immunoreactivity in anterior horns of the normal spinal cords of humans, rats and mice was primarily identified in the neurons: cytoplasmic staining was observed in almost all of the anterior horn cells. Intranuclear localization in some neurons was also observed with Prxll immunostaining using the two anti-Prxll antibodies, as previously reported [24]. Considering that endogenous Prxll and GPxl within the neuronal cytoplasm are regulators of the redox system, our finding that almost all of the normal spinal motor neurons coexpressed Prxll/GPxl confirms that these motor neurons maintain themselves utilizing the intracellular Prxll/GPxl system, that is, the redox system.

Corroborating previous findings [24], neuronal LBHIs positive for SOD1, Prxll, and GPxl were observed in both the SOD1-mutated FALS patients and the four transgenic ALS animal models expressing human mutant SOD1. A breakdown of the redox system was seen in the SOD1-mutated motor neurons containing inclusions. It is possible that the intra-inclusional co-aggregation of Prxll/GPxl with SOD1, or the sequestration of Prxll/GPxl with SOD1 into the inclusions causes the intracytoplasmic reduction of Prxll/GPxl, thereby reducing the availability of the redox system [24]. Although inclusions were seen in some motor neurons with the SOD1 gene mutation, other SOD1-mutated motor neurons progressed to the cell death without forming the inclusions.

An interesting feature was the presence of certain residual motor neurons coexpressing Prxll/GPxl throughout the ALS disease course in SALS patients and among SOD1-mutated motor neurons without inclusions. A particularly striking finding was that motor neurons overexpressing Prxll/GPxl, i.e., with redox system up-regulation, were commonly evident during the clinical courses in the divergent disease subtypes: SALS patients, SOD1-mutated FALS patients, and ALS animal models expressing human mutant SOD1.

For the SALS patients, although the number of the residual SALS motor neurons decreased with the progression of the clinical disease, some motor neurons overexpressing Prxll/GPxl were present usually up to approximately 3 years after the onset, particularly in the

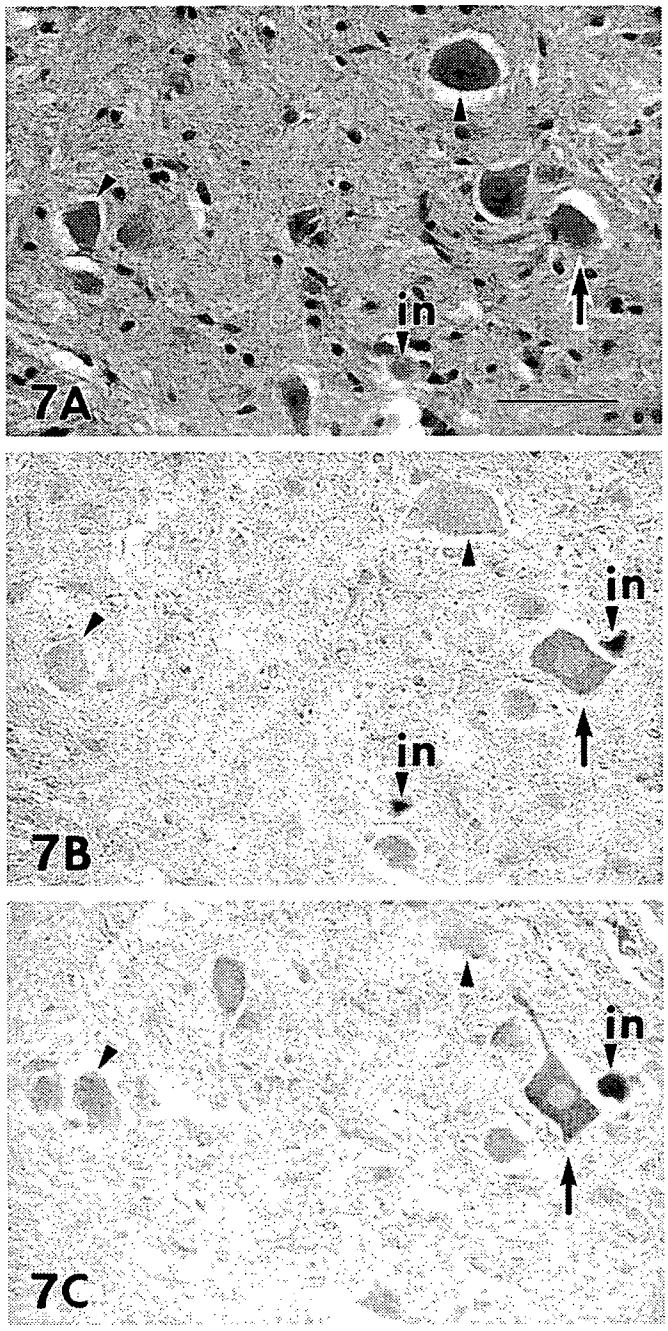

Fig. 7 Expression of Prxll and GPxl detected by immunohistochemistry in the spinal anterior horn in a G1H-G93A transgenic mouse carrying the highly overexpressed human G93A mutant SOD1 gene at 110 days of age. **A** Light microscopic preparation stained with HE. A round LBHI in the neuropil can be seen (*arrowhead* with *in*). **B** Prxll immunoreactivity of the section consecutive to that shown in **A**. **C** GPxl immunoreactivity of the section consecutive to that shown in **B**. Like in human ALS (Figs. 3, 4) and H46R rat (Fig. 6), a residual neuron overexpressing Prxll/GPxl, i.e., showing redox system up-regulation, can be observed (*arrow*). The other neurons are either faintly stained by both antibodies, or unstained (*arrowheads*), which indicates the breakdown of redox system. Round and sausage-like LBHIs in the neuropil are strongly positive for Prxll/GPxl (*arrowhead* with *in*). Observation of the HE-stained section in **A** reveals no difference between the neuron showing the redox system up-regulation (*arrow*) and the neurons exhibiting the redox system breakdown (*arrowheads*). **B, C** No counterstaining. *Bar* **A** (also for **B, C**) 50 μm

patients with no respiratory assistance. Thereafter, the number of these overexpressing motor neurons decreased dramatically as disease progressed. The immunohistochemical features are consistent with the Western blot findings that the levels of the Prxll/GPxl in the SALS patient after a clinical course of 2.5 years were almost the same levels as in normal cases in spite of loss of the motor neurons, whereas the levels decreased in the SALS patient after a clinical course of 11 years 5 months.

In the SOD1-mutated FALS patients, as in SALS patients, certain residual motor neurons without LBHIs also overexpressed Prxll/GPxl in the four short-term-surviving patients within 18 months after onset. In the ALS animal models, as in the human diseases, some residual motor neurons showed overexpression of Prxll/GPxl at 160 days of age in H46R rats, at 150 days of age in G93A rats, at 110 days of age in G1H-G93A mice and at 215 days of age in G1L-G93A mice. The presence of this common Prxll/GPxl-overexpression mechanism during the clinical course of ALS suggests that the redox system up-regulation represents one of the endogenous mechanisms that are activated by the ALS stress. At the terminal stage of ALS, however, disruption of this mechanism was observed. Although some residual ALS neurons coexpressed both proteins, while many others were negative, there was no apparent difference among these neurons on HE preparations.

In general, the redox system is one of the most crucial life supporting systems in living cells, serving as an antioxidant enzyme defense system that is synchronously linked to important physiological functions such as cellular differentiation, immune response, growth control, apoptosis, and tumor growth [4, 9, 19, 26, 31,

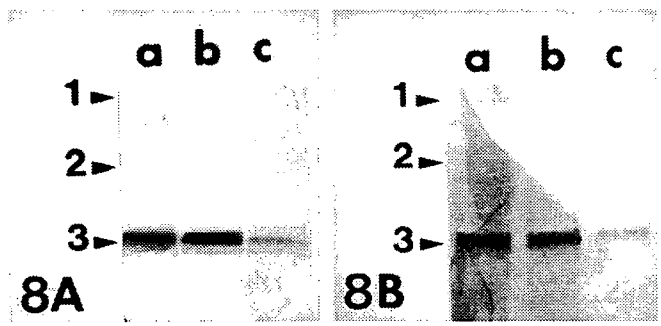

Fig. 8 Western blot analyses using the antibodies against Prxll (**A**) and GPxl (**B**). A 20-μg sample of the soluble protein extract from each sample was applied to each lane. Molecular mass markers: *1* ovalbumin (45 kDa); *2* carbonic anhydrase (31 kDa); *3* trypsin inhibitor (21.5 kDa). **A** *Lane a*: Normal control, *lane b*: an SALS patient with a clinical course of 2.5 years (case 19). *lane c*: an SALS patient with a clinical course of 11 years 5 months (case 40). A single band at approximately 23 kDa is observed in all samples. The intensity of Prxll immunoreactivity in *lane b* (ALS case 19) appears to be almost identical to that in *lane a* (normal). By contrast, Prxll expression in *lane c* (ALS case 40) appears to be lower than that in *lane a* (normal). **B** A single band of about 22 kDa is detected in each sample. Expression of GPxl in *lane b* (ALS case 19) shows almost the same intensity as that in *lane a* (normal). However, the level of GPxl expression in *lane c* (ALS case 40) is decreased below that seen in *lane a* (normal)